Geomech. Geophys. Geo-energ. Geo-resour. (2024) 10:172
https://doi.org/10.1007/s40948-024-00895-2

RESEARCH

The maximum magnitude of natural and induced earthquakes

Julian J. Bommer · James P. Verdon

Received: 15 February 2024 / Accepted: 6 October 2024
© The Author(s) 2024

Abstract A key element in the assessment of seismic hazard is estimation of the maximum possible earthquake magnitude, Mmax. A great deal of effort has been invested in developing approaches to estimate Mmax for natural (tectonic) earthquakes, especially in regions of relatively low seismicity where it is difficult to associate observed seismicity with known geological faults. In probabilistic seismic hazard analysis, there has been a tendency to assign a narrow range of large values to Mmax. This results in the impression that hazard results are insensitive to this parameter, which is not the case when the Mmax distribution captures the full range of possible values. For induced seismicity, Mmax estimates can have far-reaching implications both in terms of quantitative assessments of the resulting seismic hazard and risk, and in terms of the public and regulatory perception of this risk. Estimates of Mmax for induced seismicity need to distinguish between driven earthquakes, for which magnitudes are largely controlled by operational parameters, and triggered tectonic earthquakes, together with estimates of the likelihood of such triggering. Distributions of triggered Mmax may be limited to smaller magnitudes than distributions for natural seismicity due to the shallow depth of most injection/extraction wells. For the management of induced seismic risk, the expected largest event magnitude (which may be influenced by a Traffic Light Scheme in operation) may be more relevant than any physical upper bound truncating the recurrence relationship.

Article Highlights

- Maximum magnitude estimates for natural earthquakes are often very conservative, underestimating the influence on seismic hazard.
- For induced seismicity, need to distinguish driven from triggered earthquakes, and between expected and absolute maximum magnitudes.
- Maximum magnitudes of triggered earthquakes may be smaller than those for natural seismicity due to shallow depths of injections.

Keywords Induced seismicity · Induced earthquakes · Maximum magnitude · Triggered earthquakes · Seismic hazard analysis · Seismic risk

Supplementary Information The online version contains supplementary material available at https://doi.org/10.1007/s40948-024-00895-2.

J. J. Bommer (✉)
Dept. of Civil & Environmental Engineering, Imperial College London, London SW7 2AZ, UK
e-mail: j.bommer@imperial.ac.uk

J. P. Verdon
School of Earth Sciences, University of Bristol, Wills Memorial Building, Bristol BS8 1RJ, UK

Published online: 22 October 2024

1 Introduction

The largest possible earthquake magnitude associated with a given seismic source is a key element of epistemic uncertainty in any seismic hazard or risk assessment. Considerable effort has been invested in the estimation of the maximum magnitude for natural (i.e., tectonic) earthquakes, even though the impact of this parameter in probabilistic seismic hazard analyses (PSHA) is usually modest. For induced seismicity, on other hand, the estimation of the maximum magnitude can be a critical choice, not only for the outcomes of hazard and risk analyses but also from the perspective of perceived risk and the attendant societal and regulatory concern. Some researchers have proposed that the maximum magnitudes adopted for induced seismicity should be the same as those used for natural seismicity to account for the possibility of triggered tectonic earthquakes, but there may be reasons why such an approach could be unnecessarily and unhelpfully overconservative.

In this paper, we begin with a brief discussion of the role of maximum magnitude, or Mmax, in seismic hazard and risk assessments and summarize the approaches that have been used to estimate Mmax for natural earthquakes. We then discuss the estimation of Mmax for induced seismicity, including the crucial consideration of whether the definition of Mmax should be the same for natural and induced seismicity. We also discuss the importance of distinguishing between industrially driven versus triggered earthquakes. We provide an overview of the methods that have been proposed to estimate the maximum magnitudes of induced earthquakes, and also note how operational factors can be invoked to limit Mmax. We conclude with a discussion of how Mmax estimation should be approached for anthropogenic seismicity to balance the need to provide adequate levels of protection against the potential impacts of such earthquakes and the obstacles that can be placed on energy technologies if Mmax values are assigned with excessive precaution.

2 Mmax in seismic hazard and risk assessment

Before discussing how Mmax is estimated, we briefly discuss the purpose and definition of this parameter in the assessment of earthquake hazard and risk. Seismic hazard corresponds to the potentially damaging effects of earthquakes, such as surface fault rupture and strong ground shaking, whereas risk relates to the potential impact of these effects on the built environment and its occupants, which depends on the fragility (or degree of earthquake resistance) of the exposed buildings and infrastructure.

2.1 Deterministic seismic hazard analysis

In the historical development of seismic hazard analyses for tectonic earthquakes, a great deal of attention has been focused on estimating the magnitude of the largest possible earthquake associated with any given seismic source. In deterministic seismic hazard analysis (DSHA), in which the ground motions at the target site are calculated for one or more scenario earthquakes, the objective was to define the maximum credible earthquake, or MCE, on the premise that this would provide a safe basis for earthquake-resistant design through specification, in effect, of a worst-case scenario. However, since the distance of the earthquake from the site and the variability in the ground-motion prediction equation (GMPE) also exert influences on the amplitude of ground motion that are at least as strong as that of the magnitude, the resulting ground motions are generally not a worst-case scenario (e.g., Bommer 2003).

An important shortcoming with DSHA is that it does not provide any insight into the likelihood that the calculated motions at the site could be reached or exceeded. Consequently, it does not offer any rational basis for seismic design or risk mitigation decisions, as a result of which the use of DSHA has declined enormously since it has been replaced by probabilistic seismic hazard analysis, or PSHA, which is now widely viewed as best practice. This is not to say, however, that scenario-based hazard analysis has no place in seismic risk assessment, since such approaches can be very useful in many applications including impact assessments and emergency planning (e.g., McGuire 2001). However, the magnitudes of such scenario earthquakes are generally selected to reflect the size of events that are likely to happen within the foreseeable future rather than to represent extreme events of very low probability (e.g., EERI 2020).

2.2 Probabilistic seismic hazard analysis

Whereas DSHA considers unique combinations of magnitude (M), distance (R), and the number of standard deviations (ε) above the median prediction from the chosen GMPE, PSHA considers all possible combinations of these three variables. By including the average recurrence rates of earthquakes of different magnitude and the probability associated with each ε level (from the standard normal distribution), PSHA calculates the annual frequency of exceedance of different levels of ground shaking at the target site by integrating across all possible contributing events (Fig. 1).

Integration limits are necessarily set on all three variables (e.g., Bommer and Crowley 2017). The maximum magnitude, Mmax, is the upper limit on magnitude, and is generally defined as the largest earthquake that could occur within a given seismic source during the current tectonic regime.

For most of the PSHA inputs depicted in Fig. 1, it is usually not possible to unambiguously define the optimal model or parameter value, due to epistemic uncertainty (reflecting our lack of knowledge). Therefore, standard practice in PSHA is to determine a range of values or models, each with associated weights or probabilities reflecting the degree-of-belief in being the best estimate, and these are organized as branches in a logic-tree with a node for each model element or parameter. (e.g., Kulkarni et al. 1984; Bommer 2012). The objective of each node of the logic-tree, and indeed the logic-tree as a whole, is to capture both the best estimate and the associated epistemic uncertainty, which has been summarized as the center, body, and range of technically defensible interpretations, or CBR of TDI (USNRC 2018).

The maximum magnitude is a clear example of an epistemic uncertainty, for which there should therefore be a node in the logic-tree defining the inputs to PSHA. The nodes for Mmax in PSHA logic-trees frequently carry branches with alternative large values that are separated by less than a unit of magnitude, whence the hazard results tend to be insensitive to large values of Mmax. The purpose of the Mmax node in a logic-tree should be to capture the uncertainty associated with size of the largest earthquake that might occur and the related uncertainty regarding how much greater is this maximum than the largest earthquake that has been observed, M_{obs}. The largest historical earthquake clearly represents a lower bound on the Mmax distribution (since any

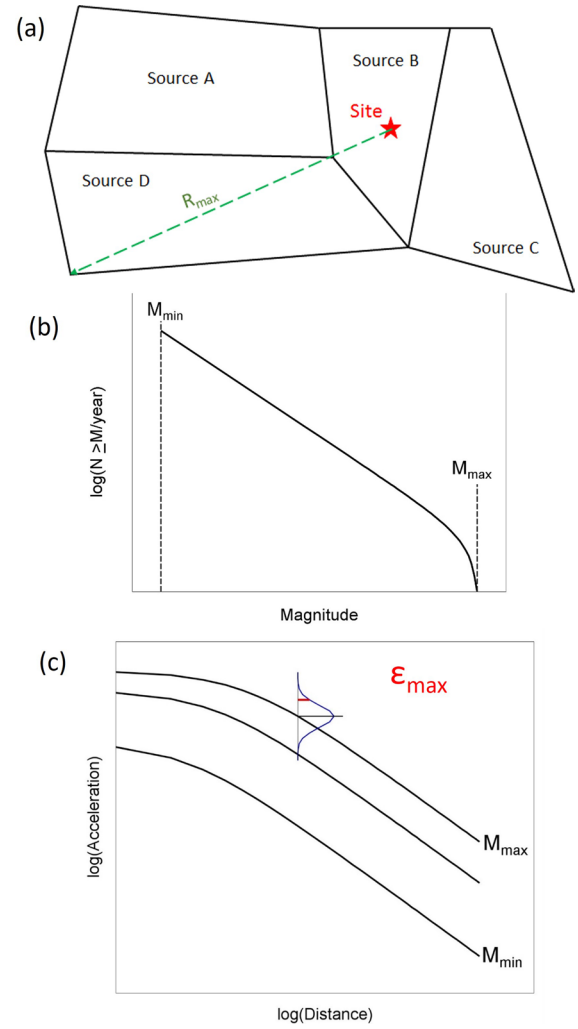

Fig. 1 Illustration of the three random variables in PSHA integrations and their limits: **a** seismic source zones that define the distribution of distances, R, at which future earthquake may occur; **b** recurrence relationships that define the average annual rates of earthquakes ≥ M; **c** GMPEs predicting distributions of ground-motion amplitudes for specified combinations of M and R (Bommer and Crowley 2017)

event that has occurred could be expected to recur at some point), possibly with a small upwards adjustment to account for uncertainty in the magnitude of that event, especially if it has been determined from macroseismic or geological data rather than modern instrumental measurements.

If the earthquake catalogue for a seismically active region covers several centuries and is long compared to the average recurrence interval of the largest earthquakes, then repeated large magnitudes may be indicative of Mmax and the increment (or rather the range of possible increments) between M_{obs} and Mmax may be small. Conversely, if the M_{obs} is relatively small, then there is likely to be a justification for a broader range of Mmax estimates. If, in such a situation, the logic-tree branches only carry large values of Mmax, the model in effect is stating that in all future scenarios, earthquakes will occur that are significantly larger (but still below Mmax) than the largest event that is known to have occurred.

The implications of this are clearest when using a Monte Carlo approach to PSHA (e.g., Musson 2000; Bourne et al. 2015), in which possible future earthquake catalogues are generated based on the recurrence parameters and seismic source geometry. Imagine a region in which the largest known earthquake had a magnitude of 5.0 and the Mmax values assigned in the logic-tree are 6.8, 7.0 and 7.2. In such a situation, every single future earthquake catalogue will include events with magnitudes above 5 and up to 6.8. If the catalogue is of short duration and considered to be temporally and/or spatially incomplete, this may seem reasonable, but it could in fact be extremely conservative if, in reality, events could not occur that are more than a small fraction larger than M_{obs}. A more appropriate distribution of Mmax would span a range that extends from slightly above M_{obs} to the largest event considered physically possible, with the shape of the distribution—and specifically whether it is skewed towards lower or higher values—reflecting the length and completeness of the earthquake catalogue and the number of events it contains with magnitudes close to M_{obs}. As explained in Sect. 3.2, these considerations are captured in the Bayesian updating approach that is widely used to estimate Mmax for PSHA in stable continental regions.

The question of how much larger than M_{obs} should Mmax be is particularly important for induced seismicity, especially if the estimates of maximum magnitude are based on the premise of triggered tectonic earthquakes whereas observations relate to seismic events that are driven by injection or extraction operations (see Sect. 4).

2.3 The importance of Mmax in seismic hazard assessments

As noted above, when logic-tree branches for Mmax span a narrow range of large magnitude values, the impact on PSHA results tends to be small since hazard estimates are generally insensitive to large magnitudes. The weak influence of large Mmax values on hazard estimates is a result of three factors: (1) the very long recurrence intervals of such large-magnitude earthquakes; (2) the saturation of ground-motion scaling at larger magnitudes; and (3) the sparse sampling from the distribution of ground-motion residuals by these infrequent events (Minson et al. 2021; Fig. 2). Understood in simple terms, the recurrence rates of large magnitude earthquakes are very low hence they do not contribute to the hazard estimates (except for low oscillator frequencies and very long return periods), and the low rates are not compensated by higher amplitudes of shaking at the site because of the nonlinear scaling of ground motion with magnitude and the fact that the degree of sampling of the aleatory distribution of residuals (i.e., the level of ε) increases with the recurrence rate of the earthquakes. An important feature to note in Fig. 2 is the shape of the recurrence curve in the left-hand plot, in which Mmax is not applied as an abrupt truncation of the log-linear Gutenberg-Richter recurrence relationship but rather as the upper limit of a taper. Such tapers are often supported by observational data and are generally applied in recurrence models for PSHA (e.g., Kagan and Jackson 2000), although there is still debate regarding the physical presence of such deviations (e.g., Main 2000) and whether these apparent truncations in the recurrence data are statistically significant (e.g., Utsu 1999). However, the

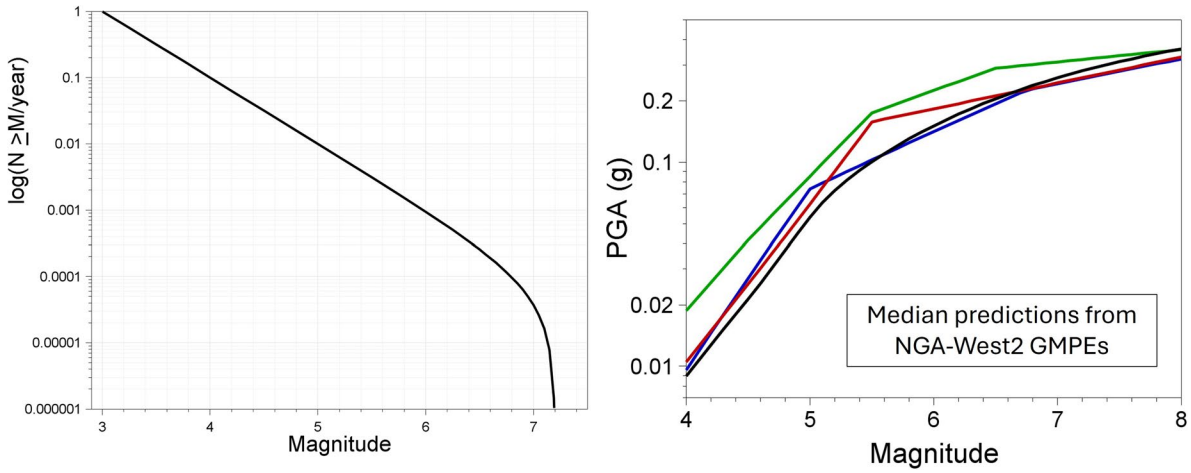

Fig. 2 Illustration of the reasons that very large magnitude earthquakes have minimal impact on the results of PSHA. Left: Typical recurrence relationship with very low recurrence rates for large-magnitude events; right: median predictions from the NGA-West2 GMPEs against magnitude, showing the saturation of magnitude scaling for larger events

focus in this paper is on the limiting values of magnitude rather than the nature of the upper end of the magnitude-frequency recurrence curve, albeit that the two topics are closely related.

If the Mmax distribution is broad, with its lower limit incrementally larger than Mobs, then the impact on the hazard results can be important (see Sect. 3.2 and Fig. 6). For induced seismicity, for which observed values of magnitude are generally small, seismic hazard (and risk) estimates will depend strongly on whether the selection of Mmax values is a broad distribution – commencing just above Mobs, when there have been extensive observations during operations, and allowing for the possibility of triggering not occurring (see Sect. 4.1) – or a narrow distribution corresponding to Mmax values for tectonic earthquakes. When there is the possibility of Mmax being low, the hazard can be greatly reduced. Figure 3 shows the Mmax logic-tree developed by Atkinson et al. (2015) for a PSHA for induced earthquakes related to hydraulic fracturing, which has its lower bound at **M** 4.5, just above the largest observed magnitude of **M** 4.4; although the logic-tree allows for a large magnitude (M 6.5) triggered tectonic event, 70% of the weight is assigned to the largest possible induced earthquake being no more than 0.6 magnitude units greater than the maximum observed event. The hazard sensitivity plot in the right-hand frame, which compares the induced seismic hazard with the results of PSHA for natural seismicity,[1] shows the dramatic effect of increasing the Mmax for induced seismicity from M 5 to M 7, resulting in an order of magnitude increase in the 10,000-year levels of ground motion.

Regardless of the impact of Mmax estimates on calculated seismic hazard, the proposed maximum magnitudes can exert a very significant influence on the perception of seismic risk due to induced seismicity. However unlikely the upper estimates assigned to this parameter may be – and even if they are therefore assigned very small weights in a logic-tree – they will often be interpreted as predictions of the largest earthquakes that could occur. From the perspective of public concern and regulatory control, the upper tail of distributions of possible Mmax values can lead to unfavorable decisions regarding energy-related operations even if the associated probabilities are very small: logic-tree weights of Mmax values will inevitably, but erroneously, be interpreted as probabilities of events of that magnitude occurring. This

[1] Inconsistencies in the PSHA input models for natural and induced seismicity used by Atkinson et al. (2015) unfavourably bias the relative impact of induced earthquakes, but a discussion of these issues is beyond the scope of this article.

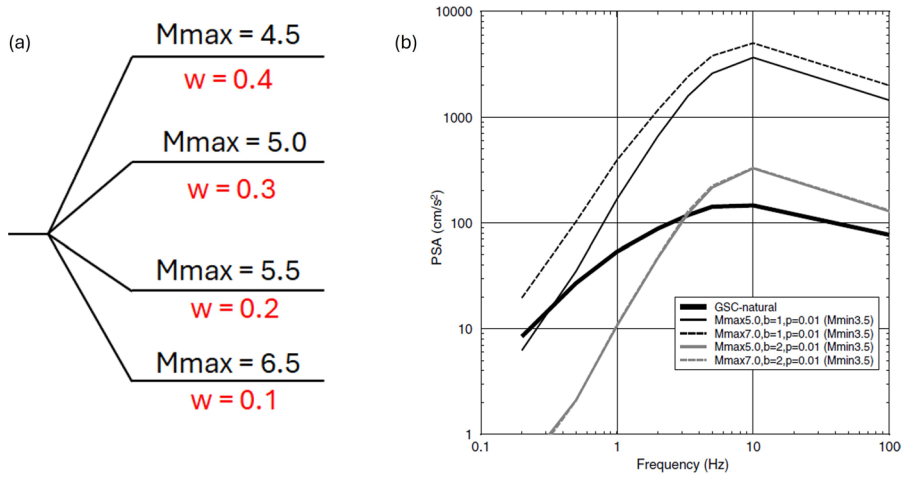

Fig. 3 **a** Logic-tree for Mmax proposed by Atkinson et al. (2015) for a PSHA for hydraulic fracturing-induced seismicity in Fox Creek, Alberta, in Canada; **b** uniform hazard response spectra for a 10,000-year return period for natural (thick black line) and induced seismicity, showing the sensitivity of the induced PSHA to alternative values of Mmax and the *b*-value, which is the slope of the recurrence curve (Atkinson et al. 2015)

means that the inclusion of such large magnitudes for potential induced events requires a strong technical justification (unless one adopts the position that such values should be included unless there is a technical basis for their exclusion, which many would not consider a rational approach to risk management).

The risk perception implications of Mmax for induced earthquakes is a serious point because in many cases of energy projects being closed down due to induced earthquakes, the cited justification has usually not been based mainly on the size of the earthquakes that did occur but rather speculation and concern about the largest earthquakes that might occur (Bommer 2022). Induced seismicity at the Groningen gas field in the Netherlands and seismicity caused by hydraulic fracturing for shale gas in the UK represent two demonstrative cases.

At Groningen the largest earthquake that has occurred was of magnitude M_L 3.6. A great deal of effort has been invested to estimate the size of the largest event that could have occurred if production had continued (Bommer et al. 2024): instead, the field has been shut-in by the Dutch government. A key factor in the justification for this decision was that the possibility of an earthquake of magnitude M 5 or larger could not be excluded. In contrast, the seismic source zone in the current European seismic hazard model that includes the Groningen region, assigns tectonic Mmax values of 6.3, 6.6 and 6.9 with weights of 0.5, 0.4 and 0.1 (Danciu et al. 2021); we are not aware of these values having caused any consternation in the Netherlands, where building regulations do not stipulate any seismic design requirements (other than for induced earthquakes in Groningen).

Following the occurrence of induced seismicity associated with hydraulic fracturing at the Preston New Road PNR-2 well in Lancashire, England, which reached a magnitude of M_L 2.9 in 2019 (Kettlety et al. 2021), the UK government imposed a moratorium on further shale gas development. The stated reason for this moratorium was the perception that "*it is not currently possible to accurately predict the probability or magnitude of earthquakes linked to fracking operations*" (BEIS 2019). The regulator had commissioned the British Geological Survey (BGS) to "*provide a site-specific estimate of the maximum magnitude of induced seismicity possible*" (OGA 2019), and the BGS chose to adopt a single value for Mmax of M 6.5 (Mancini et al. 2019). This value was adopted as it represents the most likely Mmax value for tectonic earthquakes in areas of low seismicity for the 2013 European Seismic Hazard Model (Woessner et al. 2015). The regulator inevitably interpreted this choice as implying that an M 6.5 event was possible (even if unlikely), and therefore that the potential hazard posed by allowing hydraulic fracturing to continue was unacceptable.

3 Mmax for tectonic seismicity

Although the primary motivation for this article is the estimation of Mmax for induced earthquakes, it is valuable to first review the estimation of maximum magnitudes for tectonic seismicity for three key reasons.

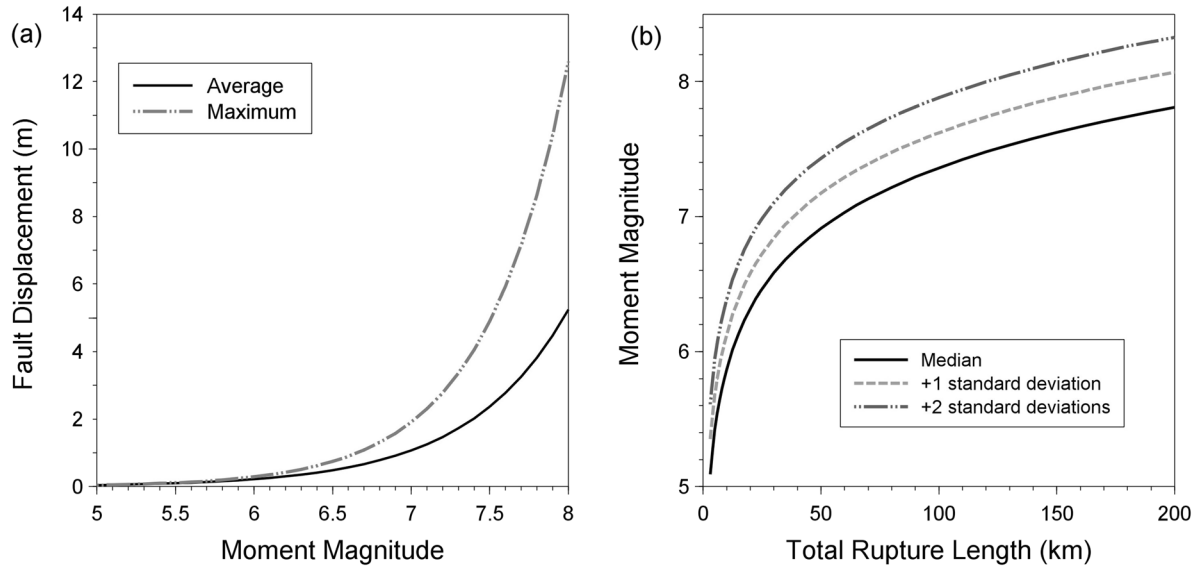

Fig. 4 Empirical scaling relationships of Wells and Coppersmith (1994) for **a** the maximum and average fault displacement as a function of magnitude, and **b** the magnitude as a function of fault rupture length and exceedance level

Firstly, a great deal of effort has been invested in developing methods for the estimation of Mmax for natural earthquakes and this body of experience is clearly of relevance. Secondly, triggered earthquakes (see Sect. 4.1) are essentially tectonic earthquakes and therefore it follows that methods used to estimate Mmax for natural earthquakes should be applicable, or at least adaptable, to induced seismicity. Finally, given the potential impact and consequences of Mmax estimates for the management of induced seismicity, it is worthwhile considering whether standard practice tends towards conservative estimates.

As noted earlier, it is very common for the Mmax node in logic-trees constructed in PSHA for tectonic earthquakes to cover a small range of large to very large magnitude values. Whereas the logic-tree is intended to capture the full range of values that could be taken by each parameter in the hazard calculations, it would often appear that the Mmax distribution is only responding to the question of how large the biggest earthquake could be without also addressing how small it might be (possibly a consequence of the adjective 'maximum' in the name of the parameter). When only a range of large values is assigned in the logic-tree, the hazard results are usually found to be very insensitive to Mmax, which in turn encourages the adoption of conservatively high maximum magnitudes because of the belief that it is not an important parameter in terms of controlling the hazard estimates. As we demonstrate below, the inference that PSHA estimates are insensitive to Mmax does not hold when broad distributions of this parameter are adopted to capture the full range of uncertainty, which suggests that more attention should be paid to constructing the Mmax node of a logic-tree. The common practice of assigning only large values is perpetuated on the basis of what appears to be a misconception, but one that is also a self-fulfilling prophecy.

3.1 Mmax for fault sources

When the sources of potential future earthquakes are represented by mapped geological faults, there is a clear technical basis for estimating the maximum magnitude. Where there are paleoseismological investigations (i.e., trenching and dating of fault offsets), the characteristic earthquake model (Schwartz and Coppersmith 1984; Youngs and Coppersmith 1985), which predicts repeated quasi-periodic events of comparable magnitude on the fault, will usually be adopted. In such cases, there will generally be a distribution of characteristic magnitudes, estimated

from empirical relationships between fault slip and magnitude, for example. The application of such relationships needs to consider variation of slip along the fault rupture and whether the observations correspond to maximum or average displacement (Fig. 4a), as well as the aleatory variability in the empirical relationships.

Estimates of Mmax for a fault source can also be obtained from empirical relationships between fault rupture dimensions and magnitude (e.g., Wells and Coppersmith 1994). There are many such empirical relationships available and the selection of the most appropriate one for any given application may be another source of epistemic uncertainty. Abrahamson (2000) proposed that Mmax should be based not on the mean magnitude obtained from these relationships but rather the upper bound prediction, which would correspond to about two standard deviations above the mean (Fig. 4b). This is a legitimate proposal for the upper limit on a Mmax distribution, but it is an extreme case (the probability of exceeding the two-sigma level is just 2.3%), and the Mmax distribution should capture the full range of possible limiting magnitudes.

Similarly, consideration needs to be given to the proportion of the measured fault length that could rupture in a single event, with some branches possibly reflecting the perfectly feasible scenario of the largest ruptures only mobilizing a certain proportion of the total length. Similar consideration needs to be given to the likelihood of multiple fault segments rupturing together in a single event and to the alternative of ruptures being limited to one or more segments. Some readers may counter that Mmax should be the largest earthquake that could ever happen and hence assuming that the entire fault length ruptures and that the corresponding magnitude should be estimated at the 97.7-percentile level from empirical scaling relationships, but we would argue that such an extreme estimate should only be the upper bound of a broader distribution that reflects physically reasonable scenarios where the largest possible earthquakes is limited to smaller values. The objective in constructing a logic-tree for PSHA should always be to capture the CBR of possible parameter values.

3.2 Mmax for distributed seismicity

Since all earthquakes are caused by rupture of geological faults, ideally all seismic sources for future seismicity would be represented by fault sources, but this is rarely, if ever, achieved in practice because of location errors in earthquake hypocenters (which hinders association with faults), lack of seismic characterization of known faults, and the fact that many faults remain undetected, especially those that do not reach the surface. Consequently, seismic source models in PSHA invariably include distributed seismicity, whether modeled as area sources or smoothed earthquake catalogues. Estimation of Mmax for such seismic sources is more challenging than for explicit fault sources. For areal source zones, Mmax is sometimes inferred from the dimensions of the largest seismogenic structures within the source although this is poor practice since it highly conservative to then assume that events of this size could occur anywhere within the source zone; indeed, when faults are explicitly modeled as sources, the maximum magnitude in the surrounding source zone should be reduced to reflect the role of the fault sources as localizing structures for the largest earthquakes.

In the absence of any identified seismogenic structures, one approach is to constrain Mmax using independently determined geodetic strain rates (e.g., Main et al. 1999). A recurrence relationship is first determined from the earthquake catalogue and then the upper limit, Mmax, is estimated such that the implied moment release rate does not exceed that obtained from geodetic measurements. Another approach used to estimate Mmax for areal source zones is adding an increment, ΔM, to the largest historical earthquake observed within the zone. In early practice ΔM was often an arbitrary value such as 0.5 but subsequently the increment was selected to reflect the length of the earthquake catalogue and the numbers of large events. In modern practice, the increase above the largest observed magnitude is calculated statistically using extreme value theory (e.g., Kijko 2004; Zentner et al. 2020); such approaches are generally viewed as requiring an extensive earthquake catalogue to work well, hence their application in site-specific PSHA studies has been rather limited.

Another approach, which has not been very widely applied in practice to date, can be adopted when there is independent geodetic constraint on the moment

release rate: the earthquake catalogue is used to determine the parameters of the Gutenberg-Richter recurrence relationship and Mmax is then calculated such that the implied moment rate matches that inferred from geodetic observations. For stable continental regions, common practice is based on the ergodic assumption whereby global observations in such regions are adopted as a substitute for long-term observations in the region of interest. A prior global distribution is constructed from the largest observed earthquakes in stable continental regions worldwide (Johnston et al. 1996a; b), to which a Bayesian update is applied using a likelihood function reflecting the largest observed earthquake in the target region and the number of events within a small interval of values below this magnitude (USNRC 2012). The likelihood function is set to zero for magnitudes below Mobs in the target region and peaks at M_{obs}; the rate at which it decays with increasing magnitude depends on the number of events in the earthquake catalogue between a defined lower threshold and M_{obs}. The posterior distribution is then renormalized and usually discretized to provide combinations of Mmax values and associated logic-tree branch weights (Fig. 5).

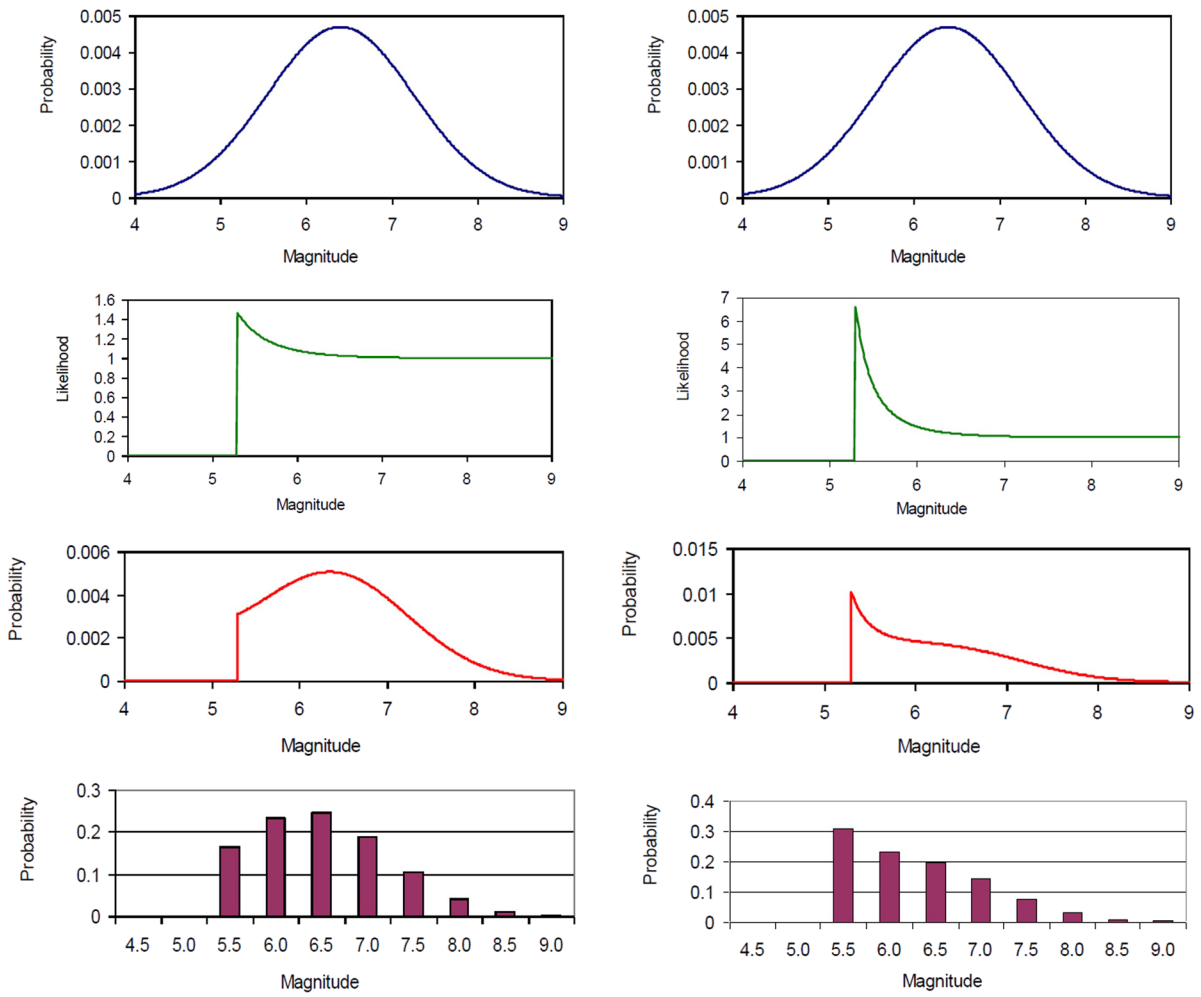

Fig. 5 Implementation of the Bayesian updating approach for Mmax using global analogues and local earthquake catalogues. Top row: prior global distribution for extended stable crust; second row: likelihood functions for local catalogue with Mobs equal to 5.3; third row: posterior distributions after application of likelihood function; bottom row: discretized versions of posterior distributions. Left-hand column for a case with two earthquakes between 4.5 and 5.3, right-hand column for the case of 10 earthquakes in this interval (modified from USNRC 2012)

Needless to say, if there had been a larger historical earthquake than the known Mobs in the catalogue, then the lower limit of the distribution may be underestimated, but this uncertainty is accommodated by the breadth of the resulting distribution.

An important and notable feature of the outcome of this approach is a broad Mmax distribution, the lower bound of which is effectively equal to the largest earthquake observed to date (or usually a value that is slightly larger as a result of the discretization). Contrary to the widely held view that seismic hazard estimates are insensitive to Mmax, when the distribution of possible values is broad—as will often be the case when the Bayesian approach is applied—the hazard results are found to vary significantly with the maximum earthquake magnitude (Fig. 6). The final output from a PSHA used in seismic risk assessment or earthquake-resistant design is generally the mean hazard curve, which is calculated as the weighted mean of annual frequencies of exceedance at each spectral acceleration level.

The upper bounds of the distributions are worthy of consideration. Updates of the global database of stable continental region earthquakes (e.g., Schulte and Mooney 2005; Wheeler 2009) have led to some reductions in the largest values but very large values are still included. Although seismic source zones are defined in absence of known faults, modern GMPEs use distances measured from extended fault ruptures, hence it is common practice to generate virtual fault ruptures for each earthquake scenario within area source zones in order to correctly calculate these distances (e.g., Bommer and Akkar 2012; Monelli et al. 2014). These distance calculations are usually performed by subroutines within PSHA codes but Bommer et al. (2023) urge practitioners to generate visualizations of the virtual fault ruptures in order to assess their consistency with the assumptions underpinning the definition of the seismic source zones (for example, for the larger magnitudes, the virtual ruptures will often exceed the dimensions of the sources). Consideration should be given, in particular, to addressing whether it is really possible that geological structures capable of generating the enormous ruptures that would be required for the largest magnitudes could be present without detection. If not, as will often be the case, the upper bounds of Mmax distributions will correspond to physically unrealizable events.

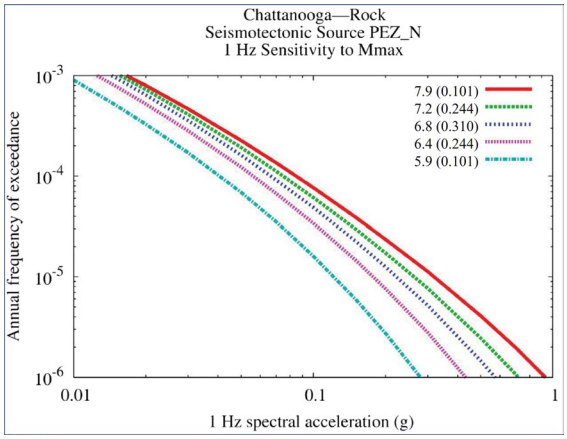

Fig. 6 Seismic hazard curves in terms of response spectral acceleration at an oscillator frequency of 1 Hz obtained with different Mmax values from a broad distribution of maximum magnitudes constructed using the Bayesian updating approach illustrated in Fig. 5 (Modified from USNRC 2012). The values in parentheses in the legend are the logic-tree branch weights

3.3 Mmax and focal depth

Seismic source models for PSHA usually include distributions of focal depths for future earthquake scenarios. These distributions are often magnitude-independent but in some cases the distributions are defined to exclude the possibility of large-magnitude earthquake scenarios initiating at very shallow hypocentral depths. In general, the sedimentary cover has lower stiffness and frictional strength, which in turn results in smaller stresses and stress drops (e.g., Vilarrasa and Carrera 2015). Also, the sedimentary cover will be younger in age, and so may contain fewer faults, which may be of shorter length. These factors combine to mean that it is far less likely, or indeed impossible, for large magnitude events to nucleate within shallow sedimentary cover. Moreover, large-magnitude events associated with shallow hypocenters would require a large rupture to initiate close to the surface and propagate mainly downwards into the crust over several kilometers, against increasing frictional strength and confining stress. While such ruptures can and do occur, they are exceptional (e.g., Mai et al. 2005) since there are physical reasons why large earthquakes generally do not initiate at shallow depths (Das and Scholz 1983). There are some notable exceptions of shallow-focus, large-magnitude earthquakes, but they correspond to either very

specific geographical regions or to triggering by large foreshocks. For example, some large earthquakes in the ancient crust of western Australia have very shallow foci (Leonard 2008), examples being the 1968 **M** 6.5 Meckering earthquake that was associated with a downward propagating fault rupture (Vogfjörd and Langston 1987) and the **M** 6.0 2016 Petermann Ranges earthquake was associated with a rupture 20 km in length confined to the top 3 km of the crust (Wang et al. 2019). An example of a naturally triggered shallow event, the 2019 **M** 7.1 Ridgecrest earthquake in California had a focal depth of just 4 km, "*implying nucleation in a zone not conducive to spontaneous, large earthquake rupture nucleation and growth*" (Lomax 2020). However, Lomax (2020) notes that this shallow hypocenter was due to stress transfer from an **M** 6.4 foreshock at 12 km depth, without which it is unlikely that the main shock rupture would have initiated at such a shallow depth.

Since most fluid injection and extraction operations leading to induced seismicity occur at shallow depths, these considerations have implications for the maximum magnitude events that could be triggered by industrial activities (see Sect. 4.3.1).

4 Mmax for induced seismicity

As noted in Sect. 2.3, the consequences of Mmax values adopted in the assessment of induced seismic hazard and risk will generally be more far-reaching than the impact of this parameter when dealing with natural (tectonic) earthquakes. We begin by discussing whether the definition of Mmax should be modified when dealing with induced seismicity, before moving on to different approaches that have been used for its estimation.

At a workshop convened by the US Geological Survey (USGS) to discuss the incorporation of induced seismicity into the US national hazard maps, "*Participants at the workshop felt that the USGS induced seismicity models should consider the possibility of triggering large regional earthquakes and should consider the same maximum magnitude distribution as was used for the tectonic earthquakes*" (Petersen et al. 2015). While the possibility of anthropogenic activities triggering tectonic earthquakes should clearly be considered, adopting the same Mmax distribution as considered in PSHA for natural seismicity may be very conservative.

The meaning of Mmax for induced seismicity may be slightly different since it could be defined as the largest earthquake that could occur during the operations plus an appropriate period for equalization of pressures and/or stresses after their completion; this distinction may be particularly important for short-lived operations that affect relatively small areas, such as hydraulic fracturing for hydrocarbon recovery and high-pressure fluid injections for enhanced geothermal systems. Some researchers have proposed that the response to the question regarding the largest earthquake to be considered when dealing with induced seismicity might be better provided by the maximum expected earthquake rather than the maximum possible earthquake (Holschneider et al. 2011; Zöller et al. 2013). We believe that there is great merit in making this distinction and we adopt the following symbology to separate the two different estimates of Mmax: Mmax^{E} for the expected maximum magnitude and Mmax^{T} for the physical upper limit that truncates the recurrence relationship. In many situations, the hazard and risk will be controlled by Mmax^{E}, particularly for operations involving short-term fluid injections such as hydraulic fracturing and enhanced geothermal systems. In such operations, and especially when a Traffic Light Scheme is implemented (see Sect. 4.5), Mmax^{E} will often be appreciably lower than Mmax^{T} (although when modelled as distributions within a logic-tree framework, they are likely to overlap). Moreover, it will often be possible to estimate Mmax^{E} with greater confidence and lower uncertainty than Mmax^{T}. At the same time, there will be situations in which Mmax^{T} may still be the appropriate limit for seismic hazard and risk analysis, a case in point being long-term, large-scale conventional hydrocarbon production, such as the Groningen field in the Netherlands (Bommer et al. 2024). Even in such situations, however, the lower end of the maximum magnitude distribution may be controlled by Mmax^{E} if seismicity rates—and hence the expected maximum magnitude (van der Elst et al. 2016)—vary with production rates.

The application of tectonic Mmax values to induced seismicity may be highly conservative because this approach ignores that possibility that only industrially driven earthquakes may occur (see Sect. 4.1 for discussion of terminology). Even if

triggered earthquakes do occur there are reasons why they may not attain the same magnitudes as earthquakes of tectonic origin. For example, tectonic estimates for Mmax assume that ruptures can nucleate at any point on any fault within the seismogenic crust, whereas induced seismicity can only occur on faults that are within sufficient proximity of the anthropogenic perturbations. For operations affecting relatively small subsurface volumes, this distinction can significantly limit the potential population of faults that could host an induced earthquake. Another factor that needs to be considered is that such operations often operate with Traffic Light Systems (TLSs), and these should serve to limit the maximum earthquake magnitude even taking account of the increases in size of trailing events that can occur following shut-in of injections (Verdon and Bommer 2021a).

Mmax estimates are often made prior to the onset of industrial operations at a site. Such a priori estimates can be based on the geomechanical characterization of a given site and the nature of the proposed operations, and may also be informed by analogous past operations of a similar nature. Induced seismicity hazard assessments from a priori characterization are often rather poorly constrained. Once a sequence of induced seismicity begins, direct characterization of the observed events often allows a much more robust hazard assessment. After defining industrially driven versus triggered tectonic earthquakes in Sect. 4.1, in Sects. 4.2 and 4.3 we examine how Mmax can be estimated during site characterization, prior to the onset of any activities. In Sect. 4.4 we go on to examine operational forecasting – how the observed induced seismicity can be used to estimate the magnitudes that might be reached during a given sequence. In Sect. 4.5 we then examine how the use of TLSs might influence Mmax estimates.

4.1 Industrially driven versus triggered earthquakes

In evaluating Mmax, it is important to make a distinction between "driven" and "triggered" seismicity. Several authors have proposed definitions of these two types of earthquake (e.g., McGarr et al. 2002; Dahm et al. 2013; Ellsworth et al. 2019). In essence, the term "triggered" earthquakes refer to the situation where the subsurface operations serve to nucleate the seismicity, but the bulk of the energy released is tectonic energy that has accumulated on faults over geological timeframes (e.g., Cesca et al. 2013). This scenario is sometimes also referred to as "runaway rupture" (e.g., Galis et al. 2017; Rodríguez-Pradilla et al. 2022), as seismogenic ruptures initiate close to the subsurface perturbation, but then "run away" along critically stressed faults away from the locus of the industrial activity. In contrast, we use the term "driven" to refer to a situation where the bulk of the energy released by the induced seismicity is directly driven by the subsurface operation itself.

Previous papers have used the terms "induced" and "triggered" to differentiate these scenarios, but this terminology creates confusion since "induced" is also used to refer collectively to all induced and triggered seismicity. We therefore adopt "driven" hereafter, leaving "induced" to refer to all earthquakes caused by human activities, regardless of their nature. While it is common to use the term induced seismicity to refer to both driven and triggered earthquakes, implying that the distinction is not important, for the estimation of maximum magnitudes it can be very important to separate the two types of induced seismic event. However, while many schemes have been proposed to discriminate induced events from natural seismicity (e.g., Verdon et al. 2019, and references therein), less attention has been given to differentiating between triggered and driven events.

One distinguishing criterion might be that triggered earthquakes will only occur on faults that are favourably orientated for slip in the in situ stress field, with a sense of motion that is consistent with the regional stress field (e.g., McNamara et al. 2015). In contrast, driven events will occur on faults that are favourably aligned with, and a sense of motion that is consistent with the deformation generated by the industrial activity in question – for example, normal faulting along the flanks of a compacting reservoir (e.g., Segall 1989), or dip-slip motions on vertical faults above a collapsing coal mine (e.g., Verdon et al. 2018).

In some studies, exceedance of the McGarr (2014) volume-based moment cap (see Sect. 4.3) has been taken as evidence of runaway rupture (e.g., Li et al. 2021; Rodríguez-Pradilla et al. 2022; McGarr and Majer, 2023), since this cap defines the maximum amount of strain that could be generated by a given subsurface volume change. Hence, if the total seismic moment released exceeds the total amount of deformation imparted by the subsurface

activity, then the implication is that the release of tectonic strain must have taken place. Indeed, McGarr and Majer (2023) explicitly state that the McGarr (2014) cap should only apply to examples of driven seismicity. However, McGarr (2014) validated his model, which is supposed to apply only to driven seismicity, with a compilation of cases that primarily consist of triggered seismicity. This, along with the confusing nature of current terminology (where "induced" is used both to refer to all anthropogenic seismicity and also specifically to driven seismicity) has seen the McGarr (2014) cap be applied to many cases where the seismicity is likely to be triggered rather than driven seismicity (e.g., Atkinson et al. 2016; Eaton and Igonin 2018).

While exceedance of the McGarr (2014) cap could be used to identify triggered rather than driven seismicity, the inverse of this situation is not true: the non-exceedance of the McGarr (2014) cap does not necessary imply that the seismicity is purely driven (i.e., is not triggered). A case of induced seismicity could be entirely releasing tectonic strain, just at a low rate such that it does not exceed the McGarr cap. In reality, some situations may be more complex, with a sequence of induced seismicity releasing both tectonic strain and strain imparted by the industrial activity in somewhat equal measure, or indeed the relative portions of tectonic and industrially driven strain release could change through time during operations (e.g., Rodríguez-Pradilla et al. 2022).

Nevertheless, from the above definitions, it is clear that Mmax estimates for driven versus triggered seismicity will require different considerations: for industrially driven earthquake sequences, Mmax will be controlled by operational factors of the causative industrial process, whereas for triggered earthquake sequences, Mmax will be controlled by tectonic factors, namely local stress conditions and the size and frictional properties of nearby faults. For practical applications, logic-trees for Mmax of induced seismicity sequences should include two nodes, the first distinguishing between the options of there being only driven earthquakes and the combination of both driven and triggered seismicity. The second logic-tree node would then develop separate branches for the range of Mmax values for both scenarios; an example of such a logic-tree is shown in Fig. 6 of Bommer et al. (2024) for the Groningen gas field.

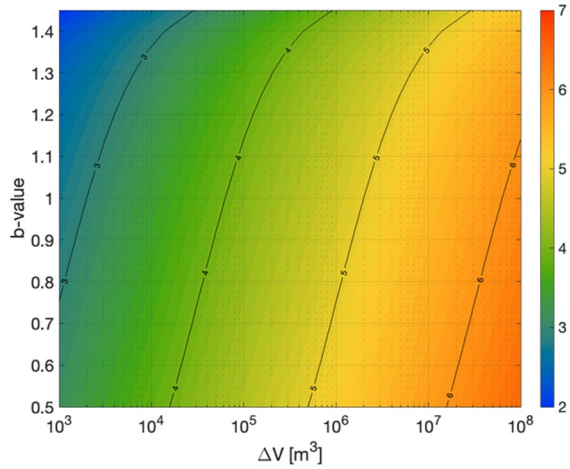

Fig. 7 Mmax as a function of volume change (ΔV) and *b*-value, based on the McGarr (2014) volume-cap (Eqs. 1–3)

4.2 Mmax for driven earthquakes

For industrially driven earthquakes, the maximum magnitude will be controlled by the amount of deformation created in the subsurface, which can be related in turn to the volume of material extracted from or added to the subsurface. McGarr (2014) showed that the cumulative seismic moment released, ΣM_O (in Nm), will be related to the volume change, ΔV (in m^3), by:

$$\Sigma M_O = 2\mu\Delta V, \tag{1}$$

where μ is the rock shear modulus. It could be assumed that Mmax corresponds to the release of the entire seismic moment as a single event, in which case:

$$Mmax = \frac{2}{3}\left(\log_{10}\Sigma M_O - 9.1\right). \tag{2}$$

However, it is more reasonable to assume that the seismic moment will be released as a sequence of events that follows the Gutenberg-Richter relationship with a given *b*-value, in which case the moment released by the largest event, $M_O max$, will be (McGarr 2014):

$$M_O max = \frac{\frac{2}{3}b}{1-\frac{2}{3}b}\Sigma M_O. \quad (3)$$

The relationship between ΔV, b, and Mmax given by Eqs. 1 – 3 is plotted in Fig. 7. Note that Eq. 3 can only be applied in cases where $b < 1.5$, though most cases of induced seismicity that we have examined have b-values close to 1 (Watkins et al. 2023).

It should be noted that, where the distinction between driven and triggered seismicity is made based on the exceedance of the McGarr (2014) cap (e.g., Li et al. 2021; Rodríguez-Pradilla et al. 2022), the above argument for Mmax is a circular one, since exceedance of this cap is taken to show that the seismicity is triggered and not driven.

The McGarr (2014) cap can produce very large estimates for Mmax for large-scale industrial activities: the cumulative injection of more than 10^7 m^3 is not uncommon for wastewater disposal wells, and the expected sequestration volumes (at reservoir temperatures and pressures) for many planned carbon capture and storage (CCS) projects exceeds this level (e.g., Verdon 2014). The McGarr (2014) cap produces Mmax values for these volumes that are larger than **M** 5.0.

In practice, much of the subsurface deformation created by industrial activities will be released aseismically, meaning that the McGarr (2014) cap usually represents a very conservative bound for Mmax for driven seismicity. As mentioned above, most of the cases that McGarr (2014) used to validate his model are widely thought to represent examples of triggered, not driven seismicity. In contrast, models of compaction for Groningen (a case where the seismicity seems to be driven) suggest that by 2023 the total subsurface volume change caused by gas extraction is 3.4×10^8 m^3. From Eqs. 1–3, the Mmax associated with this volume change is **M** 6.5. However, the largest event to have occurred at Groningen had a magnitude of **M** 3.5 (M_L 3.6).

To account for the aseismic component of deformation, Hallo et al. (2014) introduced a seismic efficiency factor, S_{EFF}, which moderates the relationship between ΣM_O and ΔV:

$$\Sigma M_O = S_{EFF}\mu\Delta V, \quad (4)$$

where S_{EFF} typically takes values that are significantly lower than 1 (e.g., Hallo et al. 2014; Verdon and Budge 2018; Verdon et al. 2024). For driven seismicity, S_{EFF} cannot exceed 1. Where a sequence of earthquakes is wholly industrially-driven (i.e., without any triggered seismicity), the magnitude defined by Eq. 4 represents the maximum possible magnitude that could be generated by the deformation in question, and therefore represents an upper-limit truncation to the Gutenberg-Richter distribution. This can be contrasted with the situation for triggered seismicity as described in Sect. 4.4.2, where the same equations can be used to estimate the maximum expected magnitude, does not necessarily imply that this value represents a truncation to the magnitude-frequency distribution.

4.3 Mmax for triggered earthquakes

As McGarr and Majer (2023) make clear, the McGarr (2014) volume-based cap should only be applied to cases of driven seismicity. For triggered seismicity, the temptation could be to simply adopt the Mmax values used in seismic hazard assessments for tectonic earthquakes in the same region, since triggered seismicity occurs on pre-existing tectonic faults, and releases tectonically accumulated strain energy. However, adopting this practice could lead to very conservative Mmax values for induced seismicity, especially if the Mmax values assigned to natural earthquakes have been generated using the widespread practice of selecting relatively large values, as discussed in Sect. 3.

Moreover, such an approach does not address the actual process of triggering by the anthropogenic processes under consideration. Triggered earthquakes will only occur on favourably oriented faults that are situated in sufficient proximity to the industrial operations, rather than on any potentially seismogenic structure in the broader region. Even when such structures are identified, estimating Mmax using empirical relationships between rupture dimensions and earthquake magnitude, such as Wells and Coppersmith (1994), implicitly assumes that rupture of the complete fault – both in terms of its length and its full width – could result from the pressure and stress changes caused by the industrial operations.

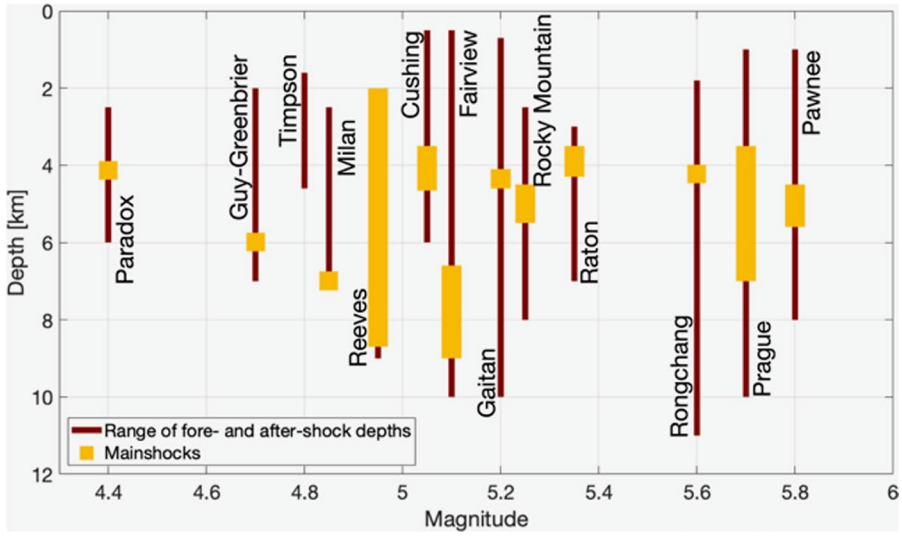

Fig. 8 Depths of mainshocks (yellow bars) and ranges of fore- and aftershock depths (red bars) for notable sequences of WWD-induced seismicity. The position of each case along the x-axis represents the magnitude of the largest event within the sequence. The yellow bars show either the range in catalogued mainshock depths or estimates of their uncertainty, and the red bars show the depth ranges for all earthquakes within each sequence. Data provided in Supplementary Material

4.3.1 Mmax and depths of induced seismicity nucleation

The overwhelming majority of subsurface industrial activities take place at shallow depths relative to the overall thickness of the seismogenic crust. Oilfield activities (and related industries such as CCS) take place in the sedimentary cover that overlies the crystalline basement. Hence, the pore pressure or geomechanical perturbations caused by these industrial activities will be limited to the sedimentary cover and perhaps the upper portion of the crystalline basement. Tectonic Mmax estimates assume that rupture can nucleate deep within the crystalline crust: this assumption will not be appropriate for most industrial activities, except in the situation where significant hydraulic or geomechanical connections (e.g., large, permeable fault structures) provide a route for perturbations to reach deep into the crust.

The issue of nucleation depths for induced seismicity versus tectonic earthquakes can be further investigated via observed cases of induced seismicity. Watkins et al. (2023) compiled a global database of case studies of wastewater disposal (WWD) induced seismicity. These cases represent most of the largest, robustly confirmed[2] examples of induced seismicity to have been monitored with networks of sufficient quality to constrain event depths. Further details for each case, including details of monitoring networks and the earthquake catalogues from which depth ranges have been computed, are provided in the Supplementary Materials.

In Fig. 8 we plot earthquake depths for induced seismicity cases in which the largest events were close to or exceeded M 4.5 and for which reliable earthquake depths are publicly available. The yellow bars represent the depths of the mainshocks (and either their location uncertainties or the range of mainshock depths reported by different studies). The red bars show the full range of depths for all events within the swarms of seismicity in each case. In most cases, these foreshocks and aftershocks delineate the fault structures that have been activated by the injection and associated perturbations.

We find a range of mainshock depths, typically from c. 4 km to nearly 10 km. However, our focus here is on the deepest depths of all earthquakes within a sequence, since these generally delineate the extent of structures activated by the anthropogenic perturbations. We find that, for all of the cases where mainshocks have exceeded **M** 5.0, the seismicity within

[2] We note that the HiQuake database of induced earthquakes (Wilson et al. 2017) lists more cases of potential induced seismicity with large magnitudes (M > 5). However, the assignation for many of the HiQuake cases as being induced is ambiguous at best, and highly dubious at worst (e.g., Bommer 2022).

Footnote 2 (continued)

We also note, however, recent work to add qualifications on these classifications based on the strength of the available evidence (Foulger et al. 2023).

the sequence extends to depths of at least 6 km, and in most cases to depths of 8–10 km. We are not aware of any cases of seismicity caused by oilfield-related activities with magnitudes $M > 5.0$ where perturbations have been limited solely to the sedimentary cover and have not penetrated a significant distance into the crystalline basement.

Clearly, structures capable of transferring shallower perturbations into the deeper crust can exist, as evidenced by the examples shown in Fig. 8. These structures might consist of permeable pathways through which elevated pore pressures are transferred to basement rocks (e.g., Hearn et al. 2018; Galloway et al. 2018; Chang and Hoon 2020), or faults on which aseismic slip creates a geomechanical stress perturbation at depth (e.g., Im and Avouac 2021). However, such structures are far from ubiquitous. For example, Verdon et al. (2016) argued that the absence of hydraulic or geomechanical connections into basement strata may account for the relative absence of induced seismicity in the Williston Basin of Saskatchewan/North Dakota, despite extensive hydraulic fracturing and wastewater disposal operations in the region. Skoumal et al. (2018a) showed that the presence of the Salina Group evaporites underlying the Marcellus Shale Formation in the Appalachian Basin provides a geomechanical and hydraulic barrier that has prevented the occurrence of induced seismicity during extensive hydraulic fracturing operations, whereas hydraulic fracturing in the co-located but deeper Utica Formation, which sits below the Salina Group, has caused significant levels of induced seismicity, with ruptures nucleating in the uppermost hundreds of metres of the basement (Friberg et al. 2014; Skoumal et al. 2015). Verdon and Rodríguez-Pradilla (2023) have shown more generally that the proximity to basement plays an important role in controlling the relative levels of induced seismicity between different shale gas plays in North America.

Where perturbations induced by oilfield activities do not penetrate any significant distance into the crystalline basement, it is clear that adopting an Mmax value from tectonic earthquakes, where it is assumed that ruptures could initiate at any depth within the seismogenic crust, will be inappropriately conservative. A more appropriate method might be to estimate an Mmax for induced events based solely on the magnitudes of tectonic events that have nucleated solely within the sedimentary cover and the uppermost basement. However, many regional earthquake catalogues do not have sufficient depth resolution to make a robust differentiation of this nature.

Green et al. (2012) based their estimate for Mmax for hydraulic fracturing of the Carboniferous Bowland Shale in northern England on previous observations of mining-induced seismicity in deep coal mines (which also target Carboniferous-age strata). Coal mining in the UK was an extensive and longstanding industry, and the deepest mines reached close to 1 km depth. Despite this, induced seismicity associated with coal mining in the UK did not exceed magnitude 3. However, Green et al.'s Mmax estimate of M 3.0 was reached during hydraulic fracturing in the Preston New Road PNR-2 well (Kettlety et al. 2021), suggesting that the Green et al. (2012) limit may not be appropriate. Importantly, most previous seismicity associated with UK coal mining seems to have been consistent with an industrially driven process (with dip-slip motions above collapsing longwall panels, e.g., Verdon et al. 2018), whereas the seismicity caused by hydraulic fracturing appears to be consistent with triggered behaviour (with strike-slip focal mechanisms that are consistent with regional stress patterns, e.g., Clarke et al. 2019; Kettlety et al. 2021). The difference between driven versus triggered behaviour may account for why coal mining in the UK never exceeded M 3.0 despite a very extensive and longstanding mining industry, whereas this magnitude was reached after hydraulic fracturing of only three wells in the Bowland Shale.

A related phenomenon to the depth of earthquake rupture is the presence of physical barriers to rupture that can limit the possible size of any induced earthquakes. Sedimentary strata often display significant vertical variability in physical and mechanical properties caused by the deposition of different lithologies. Some types of sedimentary strata, such as evaporites or clay-rich mudstones, deform in a highly ductile manner such that they form a barrier to brittle, seismogenic rupture. The presence of such layers above or below the formations being targeted by industrial activities could serve to limit the dimensions of fault ruptures, thereby limiting the size of the largest possible event. For example, induced seismicity at Groningen is observed to be constrained to within the reservoir layer (e.g., Smith et al. 2020), a fact which Boitz et al. (2024) used to estimate maximum possible rupture dimensions and thereby Mmax

values based on the thickness of the reservoir layer. Likewise, Verdon et al. (2018) identified that the maximum magnitudes of events at the Thoresby Colliery sequence were limited by the thicknesses of rock between previously mined seams below and above the working seam. These previously mined seams would since have collapsed, leaving void spaces filled with rubble that would serve to arrest any ruptures through the intact rock. We note that both the Groningen and Thoresby Colliery sequences likely represent cases of driven seismicity, but the same concept could easily be applied to observations of either driven or triggered seismicity. In practice, it may be challenging to robustly identify barriers to seismogenic rupture during site characterisation phase from which to base a priori Mmax estimates: these effects are generally identified from observations of the hypocenters of ongoing seismicity, and the observed roll-off from the anticipated Gutenberg-Richter distribution at larger magnitudes (see Sect. 4.4.1).

4.3.2 Mmax from fault stability analysis

It is common practice to identify and map the presence of faults within the subsurface at the site of a given industrial activity using geophysical methods. The orientations of faults, combined with in situ stress field measurements, can be used to evaluate fault stability or slip tendency (Morris et al. 1996), from which the sub-population of faults that are near to the Mohr–Coulomb failure criteria can be identified (e.g., Walsh and Zoback 2016; Rodríguez-Pradilla and Verdon 2024). The largest possible earthquake can then be estimated from the dimensions of the largest fault that is near to failure within the rock volume that is expected to be perturbed by the industrial activity. We note that this approach can also be used to estimate Mmax for cases of driven seismicity.

This volume analysed should be defined generously, since it may need to include not just the volume in which pore pressure change occurs, but also the volume affected by poroelastic stress changes that extend to larger distances (e.g., Deng et al. 2016; Kettlety et al. 2020; Igonin et al. 2022). Likewise, the presence of unmapped permeable pathways, such as fracture networks, can significantly increase the distance that pore pressure changes reach from a well (e.g., Igonin et al. 2021). However, only faults that are favourably orientated with respect to the in situ stress conditions – or, for cases of driven seismicity, with the nature of the induced deformation – need to be considered.

Numerical geomechanical models can also be used to directly simulate the amount of displacement (e.g., van Wees et al. 2017; Buijze et al. 2017) or stress change (e.g., Verdon et al. 2015) that will take place on predefined faults with known dimensions, from which magnitudes can be directly estimated. The challenge with this approach is that numerical geomechanical simulation tools typically have large numbers of free parameters. Model outputs can be strongly dependent on the choice of input parameter (e.g., Verdon et al. 2011), but many of the necessary parameters are poorly constrained. Where possible, models should be constrained by field observations of deformation such as observations of compaction above depleting reservoirs (e.g., Bourne and Oates 2017) or observations of uplift above a high-volume injection well (e.g., Bissell et al. 2011). Convergence between model outputs and observed deformation patterns is necessary to build confidence in model performance, but clearly that precludes the use of such models to estimate Mmax values prior to the onset of operations.

Moreover, it is often the case that when performing fault stability analyses on this basis, focus is inevitably drawn to the largest faults that are easily mappable using geophysical methods. However, induced seismicity is then found to occur along smaller faults which may not have been identified prior to operations (e.g., Nantanoi et al. 2022). Hence, whereas Mmax estimates based on fault dimensions around a given site may be less conservative than Mmax estimates taken directly from tectonic assessments, they may still be conservative relative to the seismicity that actually occurs.

4.3.3 Mmax from analogous past activities

Where large numbers of analogous activities have taken place, then observations from those operations can be used to produce a priori Mmax estimates for future operations. The definition of "analogous" could be contentious since it can be debated as to what activities represent a reasonable analogy. Verdon et al. (2016) and Verdon and Rodríguez-Pradilla (2023) have shown that the same activity

(e.g., wastewater disposal, hydraulic fracturing) can produce very different induced seismicity responses depending on the specific basin in question, and induced seismicity rates can be very different between different geological formations within the same basin (e.g., Skoumal et al. 2018a; Verdon and Bommer 2021b).

Hence, analogies should only be taken for similar activities such as injection or production of similar volumes of fluid, at similar rates/pressures, in the same geological strata. Notwithstanding this limitation, some activities now have extensive analogous data that can be used to constrain Mmax estimates. For example, many shale plays have now had thousands of wells drilled, with tens or even hundreds of thousands of individual hydraulic fracturing stages, from which rates and maximum magnitudes of induced seismicity can be established (e.g., Verdon and Rodríguez-Pradilla 2023).

As large numbers of existing analogous operations are performed (such as thousands of hydraulic fracturing wells within a given play), more data becomes available with which Mmax can be constrained using statistical methods. In situations where continuing industrial activities create a growing population of induced earthquakes, then these earthquakes can be used to populate statistical estimates for Mmax (e.g., Kijko 2004; Zöller and Holschneider 2016a). Provided that suitable analogues can be identified, there may be scope for adapting the Bayesian updating approach outlined in Sect. 3.2 for application to induced seismicity.

Observations of maximum magnitudes from analogue past operations may not represent a maximum possible magnitude (i.e., a truncation to the Gutenberg Richter distribution, $Mmax^T$). Consider a hypothetical example where maximum observed magnitudes are recorded for a large number of hydraulic fracturing wells in a particular formation. It may be that the finite injection volume for each given well produces low recurrence rates (e.g., via the seismogenic index or seismic efficiency models, see Sect. 4.4.2), such that, with small total numbers of earthquakes, larger magnitudes are not expected even if a non-truncated Gutenberg-Richter distribution is assumed. In such cases, the observed maximum magnitudes may not be informative for $Mmax^T$. Hence, when estimating $Mmax^T$ from past observations of analogue operations, consideration needs to be given to the numbers of events recorded, as well as the magnitudes of the largest events (Zöller and Holschneider 2016a).

However, observations from large numbers of analogue operations can also inform estimates of the largest expected magnitudes, $Mmax^E$, for example by defining a range of values for parameters such as the seismogenic index and seismic efficiency in order to characterise the expected behaviour at future sites (see Sect. 4.4.2). In such cases, $Mmax^E$ may represent the more important control on hazard and risk.

Where large numbers of a specific type of operation have not caused any recorded induced seismicity (as is the case for some shale gas plays where extensive hydraulic fracturing has produced no recorded induced seismicity, see Verdon and Rodríguez-Pradilla 2023), this nevertheless provides information which should contribute to Mmax estimates. In various statistical models for Mmax (e.g., Kijko 2004; Zöller and Holschneider 2016b), the number of earthquakes in the population can be replaced by the rate of seismicity multiplied by the number of years of monitoring. Similarly, for induced seismicity applications, the number of earthquakes in the population could be replaced by an expected rate of induced seismicity occurrence per well (or some other index of the rate of industrial activity) multiplied by the number of wells (or instances of the aforementioned index).

4.4 Operational estimation of Mmax

The previous sections discuss how Mmax might be assigned based on a priori evaluation of the geological conditions. Once operations begin and induced seismicity initiates, then the seismicity response can be characterised in detail, from which estimates of Mmax (as well as other key parameters such as recurrence rate) can be made. This type of approach, where observations of seismicity are made during operations and projected forwards in order to characterise the upcoming seismic hazard, is commonly used to manage induced seismicity in practice, since a priori estimates of seismic hazard are often poorly constrained except in cases where a large amount of relevant data is available. Depending on the type of approach used, some of the following methods provide estimates for $Mmax^T$, the magnitude at which the Gutenberg-Richter relationship is truncated by

some maximum physically possible earthquake size, while others provide estimates for $Mmax^E$, the maximum expected earthquake size given the finite spatial and temporal limits of human-induced subsurface perturbations, where a Gutenberg-Richter distribution is extrapolated forwards to some future finite number of events, without applying or assuming any upper limit truncation.

4.4.1 *From observed truncations of magnitude frequency distributions*

The effect of $Mmax^T$ can be seen through its impact on the frequency-magnitude distribution at magnitudes close to $Mmax^T$, since it produces a truncated upper bound, with the number of events close to $Mmax^T$ falling below that of an unbounded Gutenberg-Richter distribution. The unbounded Gutenberg-Richter distribution is modified to Burroughs and Tebbens (2002):

$$N = 10^a\left(\left[10^M\right]^{-b} - \left[10^{Mmax}\right]^{-b}\right). \quad (5)$$

In some cases, the drop-off below an unbounded Gutenberg-Richter distribution can be explicitly observed within the induced seismicity sequence, allowing $Mmax^T$ to be directly identified (e.g., Shapiro et al. 2011; Verdon et al. 2018). An example of this, from induced seismicity at the Thoresby Colliery in Nottinghamshire, England (Verdon et al. 2018), is shown in Fig. 9.

Shapiro et al. (2011) proposed that $Mmax^T$ could be estimated from the shorter axis of the ellipsoid of induced microearthquake hypocentres, on the basis that this defines the volume of influence of the injections, which in turn limits the largest circular fault rupture that could be stimulated. They argued that the $Mmax^T$ estimated from the drop-off below an unbounded Gutenberg-Richter distribution for induced events at the Soultz-sous-Forêts geothermal plant was consistent with the dimensions of the microseismic cloud.

However, in many cases where induced seismicity is observed, large events are not limited to the cloud of pre-existing microseismic events – instead, large events nucleate at the edge of the microseismic cloud and propagate outwards from this point (e.g., Kettlety et al. 2021; Igonin et al. 2022). In effect, the induced perturbation reaches a larger favourably oriented fault which then ruptures with dimensions larger than the pre-existing microseismicity. Hence, it is not widely accepted that the geometry of previous microseismic event hypocentres can be used to constrain a maximum magnitude.

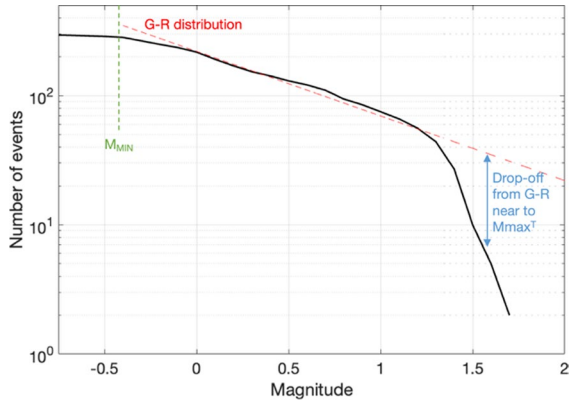

Fig. 9 Magnitude-frequency distribution for earthquakes induced by coal mining at the Thoresby Colliery, Nottinghamshire, England (black line). There is a clear drop away from the straight-line Gutenberg-Richter relationship at higher magnitudes. Note that M_{MIN} is the smallest magnitude considered in the calculation of the recurrence parameters, which is distinct from M_{min}, the smallest magnitude considered in PSHA hazard calculations. Data provided in Supplementary Material

Most cases of induced seismicity do not show clear and unambiguous evidence of a drop-off in event numbers at higher magnitudes that would indicate that magnitudes were approaching an upper truncating limit (Watkins et al. 2023; Schultz 2024). Such roll-offs only become apparent within about half a magnitude unit of $Mmax^T$ (Burroughs and Tebbens 2002) and can be difficult to robustly identify directly from statistical fitting to the observed magnitude distribution (e.g., Main 2000). Schultz (2024) proposes a method based on order statistics of magnitude jumps as a more sensitive approach to identifying whether observed magnitudes are influenced by a truncating maximum magnitude.

4.4.2 *Correlations between operational rates and seismicity*

Regardless of whether induced seismicity is driven or triggered, the rate at which seismicity occurs is expected to scale to the rate at which the subsurface is

perturbed. For a given shear stressing rate, $\dot{\tau}$, the rate of seismicity, λ, is given by (Dieterich 1994):

$$\lambda = \frac{r\dot{\tau}}{\dot{\tau}_r}, \tag{6}$$

where r is the earthquake rate at a reference stressing rate $\dot{\tau}_r$. This then implies that the rate of induced seismicity will scale linearly with the stressing rate produced by the industrial activity (Verdon et al. 2024), which in turn might be expected to scale with the rate of fluid injection or removal. As such, it is common to observe a constant scaling between seismicity and injection or production rates, even in situations where the seismicity is clearly triggered rather than driven (e.g., Dinske and Shapiro 2013; Hallo et al. 2014; Verdon et al. 2024).

This scaling is often quantified by the seismic efficiency, as defined in Eq. 4, or the seismogenic index, S_I, which relates the number of induced earthquakes, N_E, larger than a magnitude M, to the injected volume (Shapiro et al. 2010):

$$S_I = \log\left(\frac{N_E}{\Delta V}\right) + bM, \tag{7}$$

These scaling relationships can be measured during operations, and extrapolated in tandem with a planned injection or production volume to give an estimate for the cumulative seismic moment and/or the total number of seismic events that will be generated, from which $\mathrm{Mmax}^{\mathrm{E}}$ can be calculated, using Eq. 3 for a given cumulative seismic moment, while for a given number of events, $\mathrm{Mmax}^{\mathrm{E}}$ can be estimated as (van der Elst et al. 2016);

$$Mmax^E = M_{MIN} + \frac{1}{b}\log_{10} N_E, \tag{8}$$

where M_{MIN} is the minimum magnitude at which the number of events has been calculated. This type of approach has shown reasonable performance in modelling the upcoming seismicity across a broad range of induced seismicity cases (e.g., Hajati et al. 2015; Verdon and Budge 2018; Clarke et al. 2019; Kwiatek et al. 2019; Verdon et al. 2024). However, there are some examples where these methods have significantly underestimated the magnitudes of induced events (e.g., Kettlety et al. 2021; Verdon et al. 2024) – this usually happens where a new seismogenic structure begins to reactivate, and so previous events do not provide a good characterisation of the upcoming seismicity.

It should be noted that the Mmax values calculated via these methods do not represent Mmax as defined in Sect. 2, where it represents an upper bound to the Gutenberg-Richter recurrence rate (i.e., $\mathrm{Mmax}^{\mathrm{T}}$). Instead, the Mmax values using S_I and S_{EFF} as defined in Eqs. (3) represent the point at which the Gutenberg-Richter recurrence rate reaches 1. Hence, these estimates represent the maximum expected event magnitude, $\mathrm{Mmax}^{\mathrm{E}}$, not the maximum possible event magnitude. The significance of this difference is discussed further in Sect. 5. Schultz (2024) provides an estimator for the maximum expected magnitude that will be observed for a sequence where the total number of events is finite (for example, when seismicity rate scales with injection rate and the total injection volume is finite) and is also subject to a maximum possible magnitude at which the Gutenberg-Richter distribution is truncated.

The S_I and S_{EFF} methods have also been used to characterise the potential seismic hazard in advance of project development. In some cases, a reasonable distribution of S_{EFF} or S_I values can be defined, typically based on past experiences of similar operations in similar geological conditions (e.g., Verdon and Rodríguez-Pradilla 2023) – see Sect. 4.3.3 for our discussion of how Mmax can be estimated from analogue past operations. The assumed S_I and/or S_{EFF} distributions are used to estimate expected magnitude-frequency distributions based on an assumed finite injection volume, from which the largest expected magnitude size is estimated, assuming a non-truncated Gutenberg-Richter distribution.

However, where a priori estimated distributions of S_I and/or S_{EFF} are excessively broad due to a lack of relevant data to provide empirical constraint, the resulting seismic hazard assessments may be so poorly constrained as to have little practical utility (e.g., Silva et al. 2021; Bommer 2022).

4.4.3 From extreme value estimators

An alternative means of operational forecasting of induced earthquake magnitudes is using extreme value estimators, of a similar nature to those discussed in Sect. 3.2. These approaches are based on the extreme value estimators developed by Cooke (1979), which seek to estimate the likely maximum

value within a series of records, regardless of the underlying distribution from which the records are drawn. Mendecki (2016) proposed applying these methods to mining-induced seismicity, and Cao et al. (2020) adapted the Mendecki (2016) approach for seismicity induced by hydrocarbon extraction and subsurface fluid injection.

Within the overall extreme value estimator approach, there are several strategies that can be adopted for induced seismicity. The upper limit can be defined as the largest possible event within a sequence, or a jump-limited calculation can be estimated, where the largest possible magnitude jump is estimated, which is added to the largest event to have occurred to estimate Mmax (Verdon and Eisner 2024). These calculations can be performed using event magnitudes, or by using event moment or potency (moment divided by rock shear modulus).

Verdon and Eisner (2024) performed a systematic appraisal of the various extreme value estimator methods in forecasting Mmax, using a large number of induced seismicity case studies. They found that where potency values were used as input to the extreme value estimators, they produced Mmax forecasts that usually tracked the observed evolution of the induced seismicity sequences. Likewise, the "jump-limited" method using event magnitudes also tracked the observed evolution of the sequences. We note that in their study, Verdon and Eisner (2024) were using this approach to estimate the expected maximum magnitude of upcoming events (i.e., $Mmax^{E}$), and did not assume any upper-limit truncations to the Gutenberg-Richter distribution. Much like Schultz (2024), they did not identify any strong evidence for upper-limit truncations affecting the datasets used in their analysis.

4.5 Traffic light schemes and Mmax

In situations where the prior levels of constraint for recurrence rate and Mmax parameters are so broad as to be uninformative, then probabilistic approaches are not helpful. It may then be preferable to work backwards from the estimated risk to determine magnitude values that would be tolerable given the vulnerability of the exposed buildings and population (e.g., Edwards et al. 2021), and to adopt induced seismicity mitigation protocols that are designed to prevent the occurrence of larger events.

Induced seismicity is commonly regulated using Traffic Light Schemes (TLSs, e.g., Bommer et al. 2006; Verdon and Bommer 2021a). TLSs typically define a yellow-light threshold, at which operations are adjusted (e.g., reduced injection rates or pressures) to mitigate seismicity, and a red-light threshold, at which operations are terminated. TLS thresholds can be defined with respect to earthquake magnitudes or ground motion levels, although for several practical reasons, it is generally advantageous to define thresholds in terms of magnitudes, even if this are inferred from shaking levels (Bommer et al. 2006; Ader et al. 2020; Verdon and Bommer 2021a; Bommer 2022).

There has been much debate as to the efficacy of TLSs in preventing the occurrence of larger magnitude induced events (e.g., Bommer et al. 2015; Baisch et al. 2019). Van der Elst et al. (2016) argued that when an anthropogenic perturbation triggers a fault, the occurrence of seismicity is controlled by the regional tectonics. In essence, once a fault starts to be triggered, the resulting earthquakes will be sampled at random from an underlying Gutenberg-Richter distribution. If this is the case, then large events could be among the first to occur, meaning that TLSs would be ineffective for managing induced seismicity, since large events could occur with relatively little prior seismicity that could be used for mitigation. Alternatively, Verdon and Bommer (2021a) proposed that the perturbation induced by injection will grow (both in magnitude and dimension) with time, and that larger perturbations will be capable of nucleating larger events. If this is the case, we would expect induced seismicity sequences to grow sequentially as injection progresses, with larger events occurring towards the ends of the sequences. In this situation, TLSs would have the potential to mitigate large-magnitude induced events, since the earlier, lower-level seismicity can be used to guide decision-making during operations.

Verdon and Bommer (2021a) compiled a collection of hydraulic fracturing-induced seismicity cases and found statistically significant trends for large events to occur at the ends of sequences. Skoumal et al. (2018b) found similar trends for cases of hydraulic fracturing-induced seismicity in Oklahoma. Watkins et al. (2023) performed similar analyses for

sequences of wastewater disposal-induced seismicity, and again found that the distribution of largest events was not random. Unlike hydraulic fracturing-induced cases, for WWD the largest events tended to occur within the middle part of the sequences, with seismicity initially accelerating, but then tending to stabilise and then decay over longer time periods as injection continued (Verdon et al. 2024). In addition to the position of the largest events, Watkins et al. (2023) also examined the distribution of magnitude jumps within a sequence, finding a statistically significant difference in the observed distribution of jumps relative to that which would be produced by random draws from an underlying Gutenberg-Richter sequence. Instead, the observed jumps were systematically smaller, indicative of a process where magnitudes increase gradually as the sequence progresses, rather than jumping quickly from small to high magnitudes. These observations suggest that TLSs, if applied correctly, do have the ability to mitigate induced seismicity. As such, where TLSs are used to manage induced seismicity hazard, it is reasonable to assume that a requirement to stop operations at a certain threshold will have an impact on the maximum magnitude that occurs.

The role of a TLS to limit the size of the largest event will be to limit the size of the volume that is injected or produced. If a scaling is assumed between the cumulative fluid volume injected or produced and the rate of seismicity, then it becomes clear that the impact of a TLS will be to place a limit on the total number of events, and thereby the expected maximum magnitude from an unbounded Gutenberg-Richter distribution, $Mmax^{E}$. The implementation of a TLS will not serve to create a truncation to the magnitude distribution.

Moreover, TLSs are retroactive – operational decisions are made in response to the occurrence of large events. This means that the efficacy of TLSs in mitigating induced seismicity will be controlled by the size of typical magnitude jumps within induced seismicity sequences (e.g., Verdon and Bommer 2021a; Watkins et al. 2023), and the growth of magnitudes that occur during trailing seismicity (e.g., Schultz et al. 2022).

Magnitude jumps refer to the increase in magnitude for a new largest event over the previous largest event within a sequence. For example, if the previous largest event was M 3.0, and this event was followed by an M 4.0 event, this would represent a magnitude jump of 1.0. The occurrence of large magnitude jumps poses a challenge for TLSs. For example, if a TLS red-light threshold was set at M 3.0, then operations would be allowed to continue after an M 2.9 event, though some mitigation actions may have been taken if a yellow-light threshold were also in place. If this event is followed by a magnitude jump of 1.5 units, then the next large event would have a magnitude of 4.4, producing a magnitude that is significantly larger than the red-light threshold.

In some induced seismicity sequences, magnitudes have been observed to increase significantly after the end of injection (e.g., Majer et al. 2007; Ruiz-Barajas et al. 2017; Ellsworth et al. 2019; Kettlety et al. 2021). Trailing event magnitude increases can also produce events that are significantly larger than the red-light threshold at which operations are stopped.

The occurrence of large magnitude jumps and trailing increases means that the red-light limit itself does not represent the largest magnitude that induced seismicity could reach. Instead, the largest possible event that could occur under a particular TLS is given by the red-light limit, plus an additional amount that accounts for the degree to which magnitude jumps and trailing increases are expected to occur. The expected distribution of magnitude jumps and trailing increases can be estimated using statistical models (e.g., Schultz et al. 2022), or estimated empirically from observations (e.g., Verdon and Bommer 2021a; Watkins et al. 2023). Bommer and Verdon (2021a) compiled observations of magnitude jumps and trailing events from examples of hydraulic fracturing-induced seismicity around the world, finding that most magnitude jumps and trailing events were less than one magnitude unit, and the largest magnitude jump was 2.7 units. However, an important observation was that there were no cases that displayed both large magnitude jumps during the sequence and large magnitude increases for trailing events. Watkins et al. (2023) compiled observations from wastewater disposal-induced seismicity around the world, and found the largest magnitude jumps were less than 2 magnitude units (Fig. 10). These observations are consistent with the statistical models presented by Schultz et al. (2020; 2022), who also proposed a gap of 2 magnitude units between TLS thresholds and the

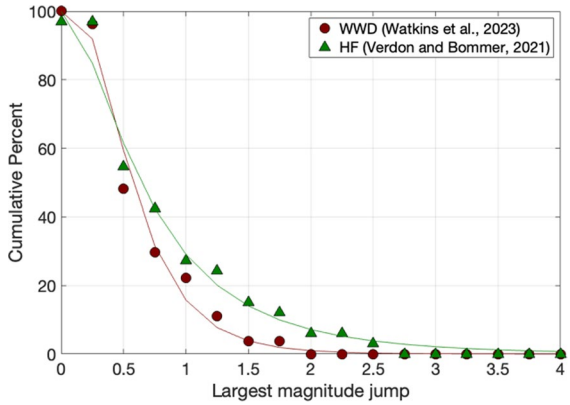

Fig. 10 Observed distributions of magnitude jumps during induced seismicity sequences caused by hydraulic fracturing (green) and wastewater disposal (red). Symbols show observed data (from Verdon and Bommer (2021a) and Watkins et al. (2023), respectively), while lines show best-fit lognormal distributions (see Watkins et al. 2023)

magnitudes they seek to prevent, in order to account for the effects of magnitude jumps and trailing events.

Based on these results, the use of TLSs should be expected to influence the expected maximum magnitudes during industrial operations. As above, the red-light value does not represent $Mmax^E$. Instead, $Mmax^E$ should be taken as the red-light value plus an additional threshold. The increment, ΔM, between the red-light threshold and the resulting $Mmax^E$ value should be inferred from the statistics of the available data – whether that be global case studies from analogous activities, as compiled by Verdon and Bommer (2021a) and Watkins et al. (2023), or datasets that are more specific to the regional geological and tectonic conditions. Observed trailing events and magnitude jumps can be used to populate a distribution of ΔM values, with $Mmax^E$ then being determined based on an acceptable probability of (non-)exceedance.

In some cases, further operations have been permitted after the occurrence of red-light events (e.g., Ellsworth et al. 2019; Kettlety et al. 2021). In these cases, the red-light limit is better thought of as a pause, rather than a permanent stop. In these cases, the levels of induced seismicity have been observed to continue from similar levels prior to the red-light pause, ultimately leading to events that were significantly larger than the red-light thresholds that were initially applied. Clearly, if TLS thresholds are to be used to define $Mmax^E$ values, then the red-light values in question need to represent the point at which operations will cease, and not merely a pause in operations.

5 Discussion

We close with a brief synthesis and discussion of the key issues and ideas that we have put forward in this article. We recognize some of the challenges for established (for natural seismicity) or emerging (for induced seismicity) practices, and hope that our proposals will prompt discussion and debate within the seismic hazard and risk community, and among operators and regulators confronting the challenges of induced seismicity in energy technologies.

5.1 Mmax for natural earthquakes

Estimating the upper bound on earthquake size in a specific region has always featured prominently as a key element of seismic hazard and risk assessment. In DSHA, which was claimed to define the worst-case scenario in terms of seismic hazard, the primary focus was usually on the estimation of the largest 'credible' earthquake, assuming that this would then lead to an upper bound on the ground shaking levels at the site (even though it is now understood that the distance from the site and the selected exceedance level of the inherent variability in the ground-motion predictions can both exert a greater influence on the site motions). Although the use of DSHA in earthquake engineering has declined significantly over recent decades, the focus on the largest possible earthquake may have influenced the perception of the maximum magnitude being a parameter of primordial importance.

In PSHA, Mmax is the upper bound of integrations across earthquake scenarios of a range of magnitudes (from the smallest events that could contribute to the risk of damage or losses), and its estimation has been the focus of a great deal of investigation and discussion.

The attention that has been given to Mmax in PSHA is, however, often not matched by its impact on the hazard estimates. When Mmax is set to a small range of high values within a logic tree, it is generally found to exert very little influence on the outcome of the PSHA calculations. The limited influence of large

Mmax values in PSHA may, consciously or otherwise, encourage the practice of assigning high estimates of the parameter; doing so allows the hazard modeler to rest in the assurance that it is very unlikely that the proposed upper limit on magnitude will be invalidated by the occurrence of an even larger earthquake.

If Mmax as defined as the largest earthquake that could possibly occur within a given seismic source (under current tectonic conditions), then fixing the maximum as the largest event that could occur under any circumstances is a reasonable response. If, however, there are any reasons why in practice the upper limit on magnitude may be limited to lower values (such as ruptures being limited to only some fraction of total fault length or the absence of large seismogenic structures within a source zone), then a distribution based only on the highest estimates is not capturing the full range of uncertainty in this parameter. The purpose and objective of constructing a logic tree is precisely to include the full range of epistemic uncertainty, not suites of conservatively biased parameter values.

If only high values of Mmax are included, and if these values are much greater than the largest earthquakes that have been observed, then the model is effectively predicting that in all future realizations of the regional seismicity there will be events of magnitudes larger than the maximum observed and of all magnitudes up to Mmax. Viewed from this perspective, Mmax estimates should usually encompass a broad range of values, the lower limit being similar to or incrementally larger than the biggest known earthquake in the seismic source, the increment depending on the length of the earthquake record and the number of events of comparable magnitude in this record. In effect, this is exactly what is often done for stable continental regions in the widely used approach based on Bayesian updating of global analogues with a likelihood function based on local observations. When broader Mmax distributions are used in PSHA, the influence of this parameter on the results can be significant.

In addition to extending the lower end of Mmax distributions to values close to the largest observed earthquakes, the upper end of the distributions may also warrant reevaluation in many cases. The prior global distributions used for stable regions, for example, have been modified at their upper limits over the years as the classification of continental regions as 'stable' has been revisited. More generally, Mmax values are often assigned to area source zones that would require fault ruptures that exceed the dimensions of the zone and, more importantly, would require enormous seismogenic structures to be present in the upper crust that have eluded detection by geologists.

5.2 Mmax for induced earthquakes

All of the preceding considerations relate to natural, or tectonic, earthquakes. We believe that it is worthwhile to revisit common practice in PSHA with respect to this parameter, both because of the potential for inappropriate conservatism, and also because these practices have clearly influenced the assessment of Mmax for induced seismicity. This is especially the case when it is argued that in the extreme, anthropogenic processes (such as the injection or extraction of fluids) could trigger incipient tectonic earthquakes and therefore Mmax values can be simply adopted from hazard studies performed for natural seismicity.

If fully probabilistic analyses of seismic hazard and risk due to induced earthquakes are to be carried out, then it is essential to develop distributions capturing the range of estimates of Mmax. A case in point is the Groningen gas field in the Netherlands, for which a probabilistic seismic risk model has been developed to enable risk levels to be compared with Dutch norms, which are expressed in terms of probabilities, and also to explore the efficacy of different risk mitigation measures (van Elk et al. 2019). In such applications, it is very important to avoid unwarranted conservatism, especially given that it is almost inevitable that some parties will interpret the Mmax estimates as predictions and the logic-tree branch weights as the associated probability of occurrence. This is not to say that legitimate estimates of larger values should be excluded for this reason, but the potential implications of the estimates should be borne in mind and values of Mmax included because there is a physical basis for postulating such scenarios (not simply invoking the precautionary principle by including such values because they cannot be definitively precluded).

Whereas for natural seismicity the relevant limit on magnitude for hazard and risk analyses will always be the physical upper bound that truncates the

recurrence relationship ($Mmax^T$), for many cases of induced seismicity, the relevant parameter will be the expected maximum magnitude, $Mmax^E$. The two definitions will sometimes be closely related and logic-tree distributions to capture their ranges of possible values will generally overlap, but for many operations, $Mmax^E$ is a more relevant, and also more tractable, quantity.

For cases where operations have been underway for some time, the Mmax distribution should begin at or just above the largest observed earthquake. This is because, once all operations have ceased and equilibrium restored, the largest event that has occurred—which will be the de facto $Mmax^E$ (but not $Mmax^T$)—must lie within the distribution that was adopted. The logic tree should also clearly identify Mmax ranges that correspond to industrially driven events and those that would represent triggered tectonic events; the weight on the latter branch should reflect the likelihood of tectonic earthquakes being triggered. Due to the relatively shallow depths of most injection/extraction wells, it will generally not be appropriate to adopt Mmax distributions developed for PSHA for natural seismicity as the node for triggered earthquakes. Bommer et al. (2024) discuss all these considerations in relation to Mmax for Groningen.

Probabilistic seismic hazard and risk analyses can only be performed when there is a body of observational data from relevant industrial operations and associated seismic monitoring, from which parameters such as recurrence rates and Mmax can be derived. The uncertainty associated with a priori estimates of seismicity rates will generally be too large for the resulting hazard and risk estimates to be informative, unless a large body of relevant analogue data has been compiled. In cases where PSHA is not a meaningful option, we propose that attempts to estimate Mmax may be neither feasible nor desirable. As our review of available approaches has shown, answers to the question regarding the largest possible magnitude of induced earthquake will carry great uncertainty but nonetheless generate levels of concern that could lead to the suspension of important energy projects.

Faced with the far-reaching consequences of highly unreliable Mmax estimates, it is preferable to invert the problem and estimate the risk that would be posed by induced earthquake scenarios of different magnitudes (e.g., Edwards et al. 2021). Locating these scenarios in the vicinity of the proposed operations and incorporating information regarding the exposed building stock and the soil or rocks on which the buildings are founded, the impact of earthquakes of different magnitude can be estimated. In this way, rather than trying to establish estimates of the largest earthquake that might occur, the focus can then move to determining the magnitude levels that would generate unacceptable risk, depending on factors including the density of population (e.g., Schultz et al. 2021).

Operational procedures can then be developed to mitigate against induced events of this size. For example, Traffic Light Schemes can be adopted, where expected distributions of magnitude jumps and trailing events can be used to set appropriate gaps between red-light thresholds and unacceptable magnitudes such that the likelihood of reaching those magnitudes is below a given level (see Sect. 4.5). Alternatively, operational earthquake forecasting methods, such as those described in Sect. 4.4, can be used to produce ongoing estimates for the largest expected event magnitude, or a probability distribution thereof. Industrial activities can then be amended or ceased if the likelihood of reaching unacceptable magnitudes exceeds a given level. A useful summary of good practice on managing the risk due to induced seismicity, including TLS, is provided by Zhou et al. (2024).

Alternatively, rather than focusing on reduction of the hazard, risk can be reduced by improving resilience. Effective public communication programs can improve the willingness of the public to tolerate felt earthquakes (Evensen et al. 2022), and engineering intervention can strengthen the weakest exposed structures in order to increase threshold magnitudes that might be considered to be unacceptable (Bommer et al. 2015).

Acknowledgements We are very grateful to editors Professor Derek Elsworth and Ranjith Pathegama for their efforts in guiding this manuscript through the review process. We would also like to express our thanks to Drs. Yihe Huang and Ryan Schultz for their constructive reviews of the manuscript, which prompted numerous changes that we believe have clarified the presentation of our ideas in this article.

Author contribution JJB and JPV both developed the ideas presented herein and contributed equally to the writing and review of the manuscript.

Funding The work of the first author has been partly funded by the Nederlandse Aardolie Maatschappij BV (NAM) in relation to the estimation of induced seismic hazard and risk for the Groningen gas field, in the Netherlands, and this assistance is gratefully acknowledged. James Verdon's contribution to this study was funded by the Natural Environment Research Council (NERC) under the SeisGreen Project (Grant No. NE/W009293/1).

Availability of data and materials The data shown in Fig. 8 are compiled from a range of publicly available sources. These are described on a site-by-site basis in our Supplementary Materials. The earthquake catalogue for the Thoresby Colliery sequence, the magnitudes of which are plotted in Fig. 9, is provided as a csv file in our supplementary materials.

Declarations

Ethics approval and consent to publication Not applicable.

Competing interests Both authors have acted as an independent consultant for a variety of organizations including hydrocarbon operating companies and governmental organizations on issues pertaining to induced seismicity. None of these organizations had any input into the conception, development, analysis or conclusions of this study.

Open Access This article is licensed under a Creative Commons Attribution 4.0 International License, which permits use, sharing, adaptation, distribution and reproduction in any medium or format, as long as you give appropriate credit to the original author(s) and the source, provide a link to the Creative Commons licence, and indicate if changes were made. The images or other third party material in this article are included in the article's Creative Commons licence, unless indicated otherwise in a credit line to the material. If material is not included in the article's Creative Commons licence and your intended use is not permitted by statutory regulation or exceeds the permitted use, you will need to obtain permission directly from the copyright holder. To view a copy of this licence, visit http://creativecommons.org/licenses/by/4.0/.

References

Abrahamson NA (2000). State of the practice of seismic hazard evaluation. In: Proceedings of GeoEng 2000, Melbourne, 19–24 November, vol. 1, pp. 659–685

Ader T, Chendorain M, Free M, Saarno T, Heikkinen P, Malin PE, Leary P, Kwiatek G, Dresen G, Bluemle F, Vuorinen T (2020) Design and implementation of a traffic light system for deep geothermal well stimulation in Finland. J Seismolog 24:991–1014

Atkinson GM, Ghofrani H, Assatourians K (2015) Impact of induced seismicity on the evaluation of seismic hazard: some preliminary considerations. Seismol Res Lett 86(3):1009–1021

Atkinson GM, Eaton DW, Ghofrani H, Walker D, Cheadle B, Schultz R, Shcherbakov R, Tiampo K, Gu J, Harrington RM, Liu Y (2016) Hydraulic fracturing and seismicity in the Western Canada sedimentary basin. Seismol Res Lett 87(3):631–647

Baisch S, Koch C, Muntendam-Bos A (2019) Traffic light systems: To what extent can induced seismicity be controlled? Seismol Res Lett 90(3):1145–1154

BEIS (2019). Government ends support for fracking: press release from the UK Department of business, energy and industrial strategy. Available at: https://www.gov.uk/government/news/government-ends-support-for-fracking last Accessed 12 Feb 2024

Bissell RC, Vasco DW, Atbi M, Hamdani M, Okwelegbe M, Goldwater MH (2011) A full field simulation of the In Salah gas production and CO_2 storage project using a coupled geomechanical and thermal fluid flow simulator. Energy Proc 4:3290–3297

Boitz N, Langenbruch C, Shapiro SA (2024) Production-induced seismicity indicates a low risk of strong earthquake in the Groningen gas field. Nat Commun 15(1):329

Bommer JJ (2003) Uncertainty about the uncertainty in seismic hazard analysis. Eng Geol 70(1–2):165–168

Bommer JJ (2012) Challenges of building logic trees for probabilistic seismic hazard analysis. Earthq Spectra 28(4):1723–1735

Bommer JJ (2022) Earthquake hazard and risk analysis for natural and induced seismicity: towards objective assessments in the face of uncertainty. Bull Earthq Eng 20(6):2825–3069

Bommer JJ, Akkar S (2012) Consistent source-to-site distance metrics in ground-motion prediction equations and seismic source models for PSHA. Earthq Spectra 28(1):1–15

Bommer JJ, Crowley H (2017) The purpose and definition of the minimum magnitude limit in PSHA calculations. Seismol Res Lett 88(4):1097–1106

Bommer JJ, Oates S, Cepeda JM, Lindholm C, Bird JF, Torres R, Marroquín G, Rivas J (2006) Control of hazard due to seismicity induced by a hot fractured rock geothermal project. Eng Geol 83:287–306

Bommer JJ, Crowley H, Pinho R (2015) A risk-mitigation approach to the management of induced seismicity. J Seismolog 19:623–646

Bommer JJ, Ake JP, Munson CG (2023) Seismic source zones for site-specific probabilistic seismic hazard analysis: the very real questions raised by virtual fault ruptures. Seismol Res Lett 94(4):1900–1911

Bommer JJ, van Elk J, Zoback MD (2024) Estimating the maximum magnitude of induced earthquakes in the Groningen gas field. Bull Seismol Soc Am. https://doi.org/10.1785/0120240054

Bourne SJ, Oates SJ (2017) Development of statistical geomechanical models for forecasting seismicity induced by gas production from the Groningen field. Neth J Geosci 96:175–182

Bourne SJ, Oates SJ, Bommer JJ, Dost B, van Elk J, Doornhof D (2015) A Monte Carlo method for probabilistic hazard assessment of induced seismicity due to conventional natural gas production. Bull Seismol Soc Am 105(3):1721–1738

Buijze L, van den Bogert PAJ, Wassing BBT, Orlic B, ten Veen J (2017) Fault reactivation mechanisms and dynamic rupture modelling of depletion-induced seismic events in a Rotliegend gas reservoir. Neth J Geosci 96:131–148

Burroughs SM, Tebbens SF (2002) The upper-truncated power law applied to earthquake cumulative frequency-magnitude distributions: evidence for a time-independent scaling parameter. Bull Seismol Soc Am 92(8):2983–2993

Cao N-T, Eisner L, Jechumtálová Z (2020) Next record-breaking magnitude for injection induced seismicity. First Break 38:53–57

Cesca S, Dost B, Oth A (2013) Preface to the special issue triggered and induced seismicity: probabilities and discrimination. J Seismol 17(1):1–4. https://doi.org/10.1007/s10950-012-9338-z

Chang KW, Yoon H (2020) Hydromechanical controls on the spatiotemporal patterns of injection-induced seismicity in different fault architecture: implication for 2013–2014 Azle earthquakes. J Geophys Res: Solid Earth. https://doi.org/10.1029/2020JB020402

Clarke H, Verdon JP, Kettlety T, Baird AF, Kendall J-M (2019) Real time imaging, forecasting and management of human-induced seismicity at Preston New Road Lancashire, England. Seismol Res Lett 90:1902–1915

Cooke P (1979) Statistical Inference for Bounds of Random Variables. Biometrica 66:367–374

Dahm T, Becker D, Bischoff M, Cesca S, Dost B, Fritschen R, Hainzl S, Klose CD, Kühn D, Lasocki S, Meier T (2013) Recommendation for the discrimination of human-related and natural seismicity. J Seismol 17:197–202

Danciu L, Nandan S, Reyes C, Basili R, Weatherill G, Beauval C, Rovida A, Vilanova S, Sesetyan K, Bard P-Y, Cotton F, Wiemer S, Giardini G (2021). The 2020 update of the European seismic hazard model: model overview. EFEHR technical report 001, v1.0.0, https://doi.org/10.12686/a15.

Das S, Scholz CH (1983) Why large earthquakes do not nucleate at shallow depths. Nature 305(5935):621–623

Deng K, Liu Y, Harrington RM (2016) Poroelastic stress triggering of the December 2013 Crooked Lake, Alberta, induced seismicity sequence. Geophys Res Lett 43:8482–8491

Dieterich J (1994) A constitutive law for rate of earthquake production and its application to earthquake clustering. J Geophys Res 99:2601–2618

Dinske C, Shapiro SA (2013) Seismotectonic state of reservoirs inferred from magnitude distributions of fluid-induced seismicity. J Seismol 17:13–25

Eaton DW, Igonin N (2018) What controls the maximum magnitude of injection-induced earthquakes? Lead Edge 37(2):135–140

Edwards B, Crowley H, Pinho R, Bommer JJ (2021) Seismic hazard and risk due to induced earthquakes at a shale gas site. Bull Seismol Soc Am 111(2):875–897

EERI (2020). San Diego earthquake planning scenario: magnitude 6.9 on the Rose Canyon Fault Zone. Earthquake engineering research institute, Oakland, CA. https://sandiego.eeri.org/

Ellsworth WL, Giardini D, Townend J, Ge S, Shimamoto T (2019) Triggering of the Pohang, Korea, earthquake (Mw 5.5) by enhanced geothermal system stimulation. Seismol Res Lett 90(5):1844–1858

Evensen D, Varley A, Whitmarsh L, Devine-Wright P, Dickie J, Bartie P, Napier H, Mosca I, Foad C, Ryder S (2022) Effect of linguistic framing and information provision on attitudes towards induced seismicity and seismicity regulation. Sci Rep 12:11239

Foulger GR, Wilkinson MW, Wilson MP, Mhana N, Tezel T, Gluyas JG (2023) Human-induced earthquakes: E-PIE: a generic tool for evaluating proposals of induced earthquakes. J Seismol 27:21–44

Friberg PA, Besana-Ostman GM, Dricker I (2014) Characterization of an earthquake sequence triggered by hydraulic fracturing in Harrison County Ohio. Seismol Res Lett 85:1295–1307

Galis M, Ampuero JP, Martin Mai P, Cappa F (2017) Induced seismicity provides insight into why earthquake ruptures stop. Sci Adv. https://doi.org/10.1126/sciadv.aap7528

Galloway E, Hauck T, Corlett H, Pană D, Schultz R (2018) Faults and associated karst collapse suggest conduits for fluid flow that influence hydraulic fracturing-induced seismicity. Proc Natl Acad Sci 115(43):E10003–E10012

Green CA, Styles P, Baptie BA (2012). Preese hall shale gas fracturing review and recommendations for induced seismic mitigation: Department of energy and climate change, London.

Hajati T, Langenbruch C, Shapiro SA (2015) A statistical model for seismic hazard assessment of hydraulic-fracturing-induced seismicity. Geophys Res Lett 42:10601–10606

Hallo M, Oprsal I, Eisner L, Ali MY (2014) Prediction of magnitude of the largest potentially induced seismic event. J Seismol 18:421–431

Hearn EH, Koltermann C, Rubinstein JL (2018) Numerical models of pore pressure and stress changes along basement faults due to wastewater injection: applications to the 2014 Milan Kansas earthquake. Geochem, Geophys, Geosyst 19:1178–1198

Holschneider M, Zöller G, Hainzl S (2011) Estimation of the maximum possible magnitude in the framework of a doubly truncated Gutenberg-Richter model. Bull Seismol Soc Am 101(4):1649–1659

Igonin N, Verdon JP, Kendall JM, Eaton DW (2021) Large-scale fracture systems are permeable pathways for fault activation during hydraulic fracturing. J Geophys Res 126:e20202JB0311

Igonin N, Verdon JP, Eaton DW (2022) Seismic anisotropy reveals stress changes around a fault as it is activated by hydraulic fracturing. Seismol Res Lett 93:1737–1752

Im K, Avouac J-P (2021) On the role of thermal stress and fluid pressure in triggering seismic and aseismic faulting at the Brawley geothermal field California. Geothermics 97:102238

Johnston AC (1996a) Seismic moment assessment of earthquakes in stable continental regions-I instrumental seismicity. Geophys J Int 124:381–414

Johnston AC (1996b) Seismic moment assessment of earthquakes in stable continental regions-11 historical seismicity. Geophys J Int 125:639–678

Kagan YY, Jackson DD (2000) Probabilistic forecasting of earthquakes. Geophys J Int 143(2):438–453

Kettlety T, Verdon JP, Werner MJ, Kendall J-M (2020) Stress transfer from opening hydraulic fractures controls the distribution of induced seismicity. J Geophys Res 125:e2019JB018794

Kettlety T, Verdon JP, Butcher A, Hampson M, Craddock L (2021) High-resolution imaging of the ML 2.9 August 2019 earthquake in Lancashire, United Kingdom, induced by hydraulic fracturing during Preston New Road PNR-2 operations. Seismol Res Lett 92:151–169

Kijko A (2004) Estimation of the maximum earthquake magnitude, m_{max}. Pure Appl Geophys 161:1655–1681

Kulkarni RB, Youngs RR, Coppersmith KJ (1984). Assessment of confidence intervals for results of seismic hazard analysis. In: Proceedings of the Eighth world conference on earthquake engineering, San Francisco, vol. 1, pp. 263-270

Kwiatek G, Saamo T, Ader T, Bluemle F, Bohnhoff M, Chendorain M, Dresen G, Heikkinen P, Kukkonen I, Leary P, Leonhardt M, Malin P, Martinez-Garzon P, Passmore K, Passmore P, Valenzuela S, Wollin C (2019) Controlling fluid-induced seismicity during a 6.1-km-deep geothermal stimulation in Finland. Sci Adv 5:eaav7224

Leonard M (2008) One hundred years of earthquake recording in Australia. Bull Seismol Soc Am 98(3):1458–1470

Li Z, Elsworth D, Wang C (2021) Constraining maximum event magnitude during injection-triggered seismicity. Nat Commun 12:1–9

Lomax A (2020) Absolute location of 2019 Ridgecrest seismicity reveals a shallow Mw 7.1 hypocenter, migrating and pulsing Mw 7.1 foreshocks, and duplex Mw 6.4 ruptures. Bull Seismol Soc Am 110(4):1845–1858

Mai PM, Spudich P, Boatwright J (2005) Hypocenter locations in finite-source rupture models. Bull Seismol Soc Am 95(3):965–980

Main I (2000) Apparent breaks in scaling in the earthquake cumulative frequency-magnitude distribution: fact or artifact? Bull Seismol Soc Am 90:86–97

Main I, Irving D, Musson R, Reading A (1999) Constraints on the frequency: magnitude relation and maximum magnitudes in the UK from observed seismicity and glacio-isostatic recovery rates. Geophys J Int 137(2):535–550

Majer EL, Baria R, Stark M, Oates S, Bommer J, Smith B, Asanuma H (2007) Induced seismicity associated with enhanced geothermal systems. Geothermics 36(3):185–222

Mancini S, Segou M, Werner MJ, Baptie BJ (2019). Statistical modelling of the Preston new road seismicity: towards probabilistic forecasting tools: British geological survey commissioned report, CR/19/068. Available at: https://www.nstauthority.co.uk/media/6147/bgs-innovations-in-forecasting.pdf last Accessed 12 Feb 2024).

McGarr A (2014) Maximum magnitude earthquakes induced by fluid injection. J Geophys Res: Solid Earth 119(2):1008–1019

McGarr A, Majer EL (2023) The 2017 Pohang, South Korea, Mw 5.4 main shock was either natural or triggered, but not induced. Geothermics 107:102612

McGarr A, Simpson D, Seeber L (2002) Case histories of induced and triggered seismicity. In: Lee WHK, Kanamori H, Jennings PC, Kisslinger C (eds) International Geophysics Series, vol 81. Academic Press, New York, pp 647–664

McGuire RK (2001) Deterministic versus probabilistic earthquake hazards and risks. Soil Dyn Earthq Eng 21(5):377–384

McNamara DE, Benz HM, Herrmann RB, Bergman EA, Earle P, Holland A, Baldwin R, Gassner A (2015) Earthquake hypocenters and focal mechanisms in central Oklahoma reveal a complex system of reactivated subsurface strike-slip faulting. Geophys Res Lett 42:2742–2749

Mendecki AJ (2016) Mine seismology reference book. Institute of mine seismology, Somerset West, South Africa.

Minson SE, Baltay AS, Cochran ES, McBride SK, Milner KR (2021) Shaking is almost always a surprise: the earthquakes that produce significant ground motion. Seismol Res Lett 92(1):460–468

Monelli D, Pagani M, Weatherill G, Danciu L, Garcia J (2014) Modeling distributed seismicity for probabilistic seismic-hazard analysis: Implementation and insights with the OpenQuake engine. Bull Seismol Soc Am 104(4):1636–1649

Morris A, Ferrill DA, Henderson DB (1996) Slip-tendency analysis and fault reactivation. Geology 24(3):275–278

Musson RM (2000) The use of Monte Carlo simulations for seismic hazard assessment in the UK. Ann Geofis 43(1):1–9

Nantanoi S, Rodríguez-Pradilla G, Verdon JP (2022) 3D-Seismic interpretation and fault slip potential analysis from hydraulic fracturing in the Bowland Shale, UK. Pet Geosci 28:petgeo2021–petgeo2057

OGA 2019. Interim report of the scientific analysis of data gathered from Cuadrilla's operations at Preston New Road: oil and gas authority, London. Available at: https://www.nstauthority.co.uk/media/6149/summary-of-pnr1z-interim-reports.pdf last Accessed 12 Feb 2024

Petersen MD, Mueller CS, Moschetti MP, Hoover SM, Rubinstein JL, Llenos AL, Michael AJ, Ellsworth WL, McGarr AF, Holland AA, Anderson JG (2015). Incorporating induced seismicity in the 2014 United States national seismic hazard model: results of 2014 workshop and sensitivity studies. USGS Open-File Report 2015–1070, US Geological Survey, Reston, VA

Rodríguez-Pradilla G, Verdon JP (2024) Quantifying the variability in fault density across the UK Bowland Shale with implications for induced seismicity hazard. Geomech Energy Environ 38:100534

Rodríguez-Pradilla G, Eaton DW, Verdon JP (2022) Basin-scale multi-decadal analysis of hydraulic fracturing and seismicity in western Canada shows non-recurrence of induced runaway fault rupture. Sci Rep 12:14463

Ruiz-Barajas S, Sharma N, Convertito V, Zollo A, Benito B (2017) Temporal evolution of a seismic sequence induced by a gas injection in the eastern coast of Spain. Sci Rep 7:2901

Schulte SM, Mooney WD (2005) An updated global earthquake catalogue for stable continental regions: reassessing the correlation with ancient rifts. Geophys J Int 161(3):707–721

Schultz R (2024) Inferring maximum magnitudes from the ordered sequence of large earthquakes. Phil Trans A 382(2270):202301853

Schultz R, Beroza G, Ellsworth W, Baker J (2020) Risk-informed recommendations for managing hydraulic fracturing-induced seismicity via traffic light protocols. Bull Seismol Soc Am 110:2411–2422

Schultz R, Beroza GC, Ellsworth WL (2021) A risk-based approach for managing hydraulic fracturing-induced seismicity. Science 372(6541):504–507

Schultz R, Ellsworth WL, Beroza GC (2022) Statistical bounds on how induced seismicity stops. Sci Rep 12:1184

Schwartz DP, Coppersmith KJ (1984) Fault behavior and characteristic earthquakes: examples from the Wasatch and San Andreas fault zones. J Geophys Res: Solid Earth 89(B7):5681–5698

Segall P (1989) Earthquakes triggered by fluid extraction. Geology 17(10):942–946

Shapiro SA, Dinske C, Langenbruch C, Wenzel F (2010) Seismogenic index and magnitude probability of earthquakes induced during reservoir fluid stimulations. Lead Edge 29(3):304–309

Shapiro SA, Krüger OS, Dinske C, Langenbruch C (2011) Magnitudes of induced earthquakes and geometric scales of fluid-stimulated rock volumes. Geophysics 76(6):WC55–WC63

Silva AH, Pita GL, Inaudi JA, Vieira LCM (2021) Induced earthquake damage assessment methodology for potential hydraulic fracturing sites: application to Manaus. Braz Earthq Spectra 37(1):180–203

Skoumal RJ, Brudzinski MR, Currie BS (2015) Earthquakes induced by hydraulic fracturing in Poland Township, Ohio. Bull Seismol Soc Am 105:189–197

Skoumal RJ, Brudzinski MR, Currie BS (2018a) Precambrian basement affects the likelihood of induced seismicity in the Appalachian Illinois, and Williston Basins, Central and Eastern United States. Geosphere 14:1365–1379

Skoumal RJ, Ries R, Brudzinski MR, Barbour AJ, Currie BS (2018b) Earthquakes induced by hydraulic fracturing are pervasive in Oklahoma. J Geophys Res 123:10918–10935

Smith JD, White RS, Avouac JP, Bourne S (2020) Probabilistic earthquake locations of induced seismicity in the Groningen region, the Netherlands. Geophys J Int 222(1):507–516

USNRC (2012). Technical report: central and eastern United States seismic source characterization for nuclear facilities. NUREG-2115, U.S. Nuclear regulatory commission, Washington D.C.

USNRC (2018). Updated implementation guidelines for SSHAC hazard studies. NUREG-2213, U.S. Nuclear regulatory commission, Washington D.C.

Utsu T (1999) Representation and analysis of earthquake size distribution: a historical review and some new approaches. Pure Appl Geophys 155:509–535

van der Elst NJ, Page MT, Weiser DA, Goebel T, Hosseini SM (2016) Induced earthquake magnitudes are as large as (statistically) expected. J Geophys Res: Solid Earth 121(6):4575–4590

van Elk J, Bourne SJ, Oates SJ, Bommer JJ, Pinho R, Crowley H (2019) A probabilistic model to evaluate options for mitigating induced seismic risk. Earthq Spectra 35(2):537–564

van Wees J-D, Osinga S, van Thienen-Visser K, Fokker PA (2017) Reservoir creep and induced seismicity: inferences from geomechanical modeling of gas depletion in the Groningen field. Geophys J Int 212:1487–1497

Verdon JP (2014) Significance for secure CO_2 storage of earthquakes induced by fluid injection. Environ Res Lett 9:064022

Verdon JP, Bommer JJ (2021a) Green, yellow, red, or out of the blue? An assessment of traffic light schemes to mitigate the impact of hydraulic fracturing-induced seismicity. J Seismol 25:301–326

Verdon JP, Bommer JJ (2021b) Comment on activation rate of seismicity for hydraulic fracture wells in the Western Canadian sedimentary basin by Ghofrani and Atkinson (2020). Bull Seismol Soc Am 111:3459–3474

Verdon JP, Budge J (2018) Examining the capability of statistical models to mitigate induced seismicity during hydraulic fracturing of shale gas reservoirs. Bull Seismol Soc Am 108:690–701

Verdon JP, Eisner L (2024) An empirically constrained forecasting strategy for induced earthquake magnitudes using extreme value theory. Seismol Res Lett. https://doi.org/10.1785/0220240061

Verdon JP, Rodríguez-Pradilla G (2023) Assessing the variability in hydraulic fracturing-induced seismicity occurrence between North American shale plays. Tectonophysics 859:229898

Verdon JP, Kendall J-M, White DJ, Angus DA (2011) Linking microseismic event observations with geomechanical models to minimise the risks of storing CO_2 in geological formations. Earth Planet Sci Lett 305:143–152

Verdon JP, Stork AL, Bissell RC, Bond CE, Werner MJ (2015) Simulation of seismic events induced by CO_2 injection at In Salah, Algeria. Earth Planet Sci Lett 426:118–129

Verdon JP, Kendall J-M, Horleston AC, Stork AL (2016) Subsurface fluid injection and induced seismicity in southeast Saskatchewan. Int J Greenhouse Gas Control 54:429–440

Verdon JP, Kendall J-M, Butcher A, Luckett R, Baptie BJ (2018) Seismicity induced by longwall coal mining at the thoresby Colliery, Nottinghamshire, UK. Geophys J Int 212:942–954

Verdon JP, Baptie BJ, Bommer JJ (2019) An improved framework for discriminating seismicity induced by industrial activities from natural earthquakes. Seismol Res Lett 90(4):1592–1611

Verdon JP, Pullen B, Rodríguez-Pradilla G (2024) Growth and stabilisation of induced seismicity rates during long-term, low pressure fluid injection. Phil Trans R S A 382:20230183

Vilarrasa V, Carrera J (2015) Geologic carbon storage is unlikely to trigger large earthquakes and reactivate faults through which CO_2 could leak. Proc Natl Acad Sci 112:5938–5943

Vogfjörd KS, Langston CA (1987) The Meckering earthquake of 14 October 1968: A possible downward propagating rupture. Bull Seismol Soc Am 77(5):1558–1578

Walsh FR, Zoback MD (2016) Probabilistic assessment of potential fault slip related to injection-induced earthquakes: application to north-central Oklahoma, USA. Geology 44(12):991–994

Wang S, Xu W, Xu C, Yin Z, Bürgmann R, Liu L, Jiang G (2019) Changes in groundwater level possibly encourage shallow earthquakes in central Australia: the 2016 Petermann ranges earthquake. Geophys Res Lett 46(6):3189–3198

Watkins TJM, Verdon JP, Rodríguez-Pradilla G (2023) The temporal evolution of induced seismicity sequences generated by long-term, low pressure fluid injection. J Seismolog 27:243–259

Wells DL, Coppersmith KJ (1994) New empirical relationships among magnitude, rupture length, rupture width, rupture area, and surface displacement. Bull Seismol Soc Am 84(4):974–1002

Wheeler RL (2009). Methods of Mmax estimation east of the Rocky Mountains. USGS Open-File Report 2009–1018, US Geological Survey, Reston, VA

Wilson MP, Foulger GR, Gluyas JG, Davies RJ, Julian BR (2017) HiQuake: the human-induced earthquake database. Seismol Res Lett 88:1560–1565

Woessner J, Danciu L, Giardini D, Crowley H, Cotton F, Grünthal G, Valensise G, Arvidsson R, Basili R, Demircioglu MB, Hiemer D (2015) The 2013 European seismic hazard model: key components and results. Bull Earthq Eng 13:3553–3596

Youngs RR, Coppersmith KJ (1985) Implications of fault slip rates and earthquake recurrence models to probabilistic seismic hazard estimates. Bull Seismol Soc Am 75(4):939–964

Zentner I, Ameri G, Viallet E (2020) Bayesian estimation of the maximum magnitude m_{max} based on the extreme value distribution for probabilistic seismic hazard analyses. Pure Appl Geophys 177(12):5643–5660

Zhou W, Lanza F, Grigoratos I, Schultz R, Crousse J, Trutnevyte E, Muntendam-Bos A, Wiemer S (2024) Managing induced seismicity risks for enhanced geothermal systems: a good practice guide. Rev Geophys. https://doi.org/10.1029/2024RG000849

Zöller G, Holschneider M (2016a) The maximum possible and the maximum expected earthquake magnitude for production-induced earthquakes at the gas field in Groningen, The Netherlands. Bull Seismol Soc Am 106(6):2917–2921

Zöller G, Holschneider M (2016b) The earthquake history in a fault zone tells us almost nothing about m_{max}. Seismol Res Lett 87(1):132–137

Zöller G, Holschneider M, Hainzl S (2013) The maximum earthquake magnitude in a time horizon: theory and case studies. Bull Seismol Soc Am 103(2A):860–875

Publisher's Note Springer Nature remains neutral with regard to jurisdictional claims in published maps and institutional affiliations.